Novel Positive Allosteric Modulators of the Human α7 Nicotinic Acetylcholine Receptor

ARTICLE *in* BIOCHEMISTRY · JUNE 2011

Impact Factor: 3.02 · DOI: 10.1021/bi102001m · Source: PubMed

6 AUTHORS, INCLUDING:

Dominik Feuerbach
Novartis Institutes for BioMedical Research
63 PUBLICATIONS **1,181** CITATIONS
SEE PROFILE

Dong-Qing Wei
Shanghai Jiao Tong University
225 PUBLICATIONS **4,773** CITATIONS
SEE PROFILE

BIOCHEMISTRY
including biophysical chemistry & molecular biology

ARTICLE

pubs.acs.org/biochemistry

Novel Positive Allosteric Modulators of the Human α7 Nicotinic Acetylcholine Receptor

Hugo R. Arias,[‡] Ruo-Xu Gu,[†] Dominik Feuerbach,[§] Bao-Bao Guo,[∥] Yong Ye,[∥] and Dong-Qing Wei*[,†]

[†]Luc Montagnier BioMedical Research Institute and National Key Laboratory of Microbial Metabolism, College of Life Sciences and Biotechnology, Shanghai Jiao Tong University, Shanghai, China

[‡]Department of Pharmaceutical Sciences, College of Pharmacy, Midwestern University, Glendale, Arizona 85308, United States

[§]Neuroscience Research, Novartis Institutes for Biomedical Research, Basel, Switzerland

[∥]Laboratory of Chemical Biology, Department of Chemistry, Zhengzhou University, Zhengzhou, Henan, China

Supporting Information

ABSTRACT: The pharmacological activity of a series of novel amide derivatives was characterized on several nicotinic acetylcholine receptors (AChRs). Ca^{2+} influx results indicate that these compounds are not agonists of the human (h) α4β2, α3β4, α7, and α1β1γδ AChRs; compounds **2**−**4** are specific positive allosteric modulators (PAMs) of hα7 AChRs, whereas compounds **1**−**4**, **7**, and **12** are noncompetitive antagonists of the other AChRs. Radioligand binding results indicate that PAMs do not inhibit binding of [^{3}H]methyllycaconitine but enhance binding of [^{3}H]epibatidine to hα7 AChRs, indicating that these compounds do not directly, but allosterically, interact with the hα7 agonist sites. Additional competition binding results indicate that the antagonistic action mediated by these compounds is produced by direct interaction with neither the phencyclidine site in the *Torpedo* AChR ion channel nor the imipramine and the agonist sites in the hα4β2 and hα3β4 AChRs. Molecular dynamics and docking results suggest that the binding site for compounds **2**−**4** is mainly located in the inner β-sheet of the hα7−α7 interface, ∼12 Å from the agonist locus. Hydrogen bond interactions between the amide group of the PAMs and the hα7 AChR binding site are found to be critical for their activity. The dual PAM and antagonistic activities elicited by compounds **2**−**4** might be therapeutically important.

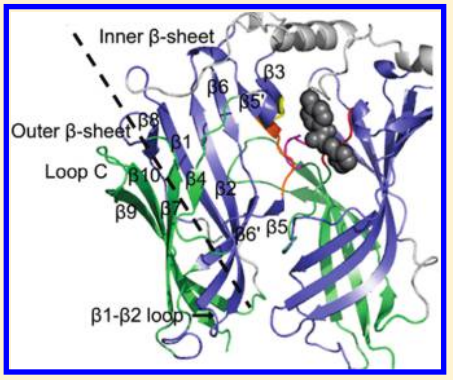

The nicotinic acetylcholine receptor (AChR) family is genetically and structurally related to the Cys-loop ligand-gated ion channel superfamily that also includes the glycine, type 3 serotonin (5-HT), and type A and C GABA receptors (reviewed in refs 1−3). AChRs are pentameric structures that can be formed by just one subunit subtype, the so-called homomeric receptors (e.g., α7, α8, and α9), or by more than one subunit subtype, the so-called heteromeric receptors (e.g., α4β2, α3β4, etc.). Neuronal heteromeric AChRs can be formed by combinations of three [e.g., $(\alpha4)_2\alpha5(\beta2)_2$] or even four (e.g., α4α6β2β3) different subunits (reviewed in ref 4), but there is no evidence of a receptor subtype formed by five different subunits. The variability of AChR subtypes permits a wide range of ligand sensitivities producing pleiotropic pharmacological effects throughout the body.

In the past 60 years, a vast amount of evidence indicates that AChRs are important for the homeostasis and function of our body. In the nervous system, for instance, presynaptic AChRs regulate the release of several neurotransmitters, including norepinephrine, 5-HT, acetylcholine (ACh), dopamine, glutamate, and GABA (reviewed in refs 1−3). In non-neuronal tissues, AChRs modulate angiogenesis and immune responses (reviewed in refs 5 and 6). In this regard, AChRs are involved in several physiologically relevant functions such as cognition, memory, pain perception, auditory response, muscle contraction, angiogenesis, and immune response. The malfunctioning of AChRs (e.g., by AChR mutations or by the activity of endogenous ligands) or the decrease in the number of AChRs (e.g., by autoantibodies) may trigger the progress of several diseases, including Alzheimer's and Parkinson's diseases, schizophrenia, Tourette's syndrome, attention deficit hyperactivity disorder, autosomal dominant nocturnal lobe epilepsy, myasthenia gravis and several congenital myasthenic syndromes, drug and nicotine addictions, anxiety and depression, pain-related diseases, immunological and inflammation problems, and tumor growth.

Because the malfunctioning of AChRs seems to be the basis for various neurological and non-neurological disorders, several laboratories have placed an emphasis on the characterization of agonists and competitive antagonists with high receptor specificity. In addition to agonists and competitive antagonists, several ligands have been synthesized and pharmacologically characterized as positive allosteric modulators (PAMs)

Received: December 20, 2010
Revised: April 20, 2011
Published: April 21, 2011

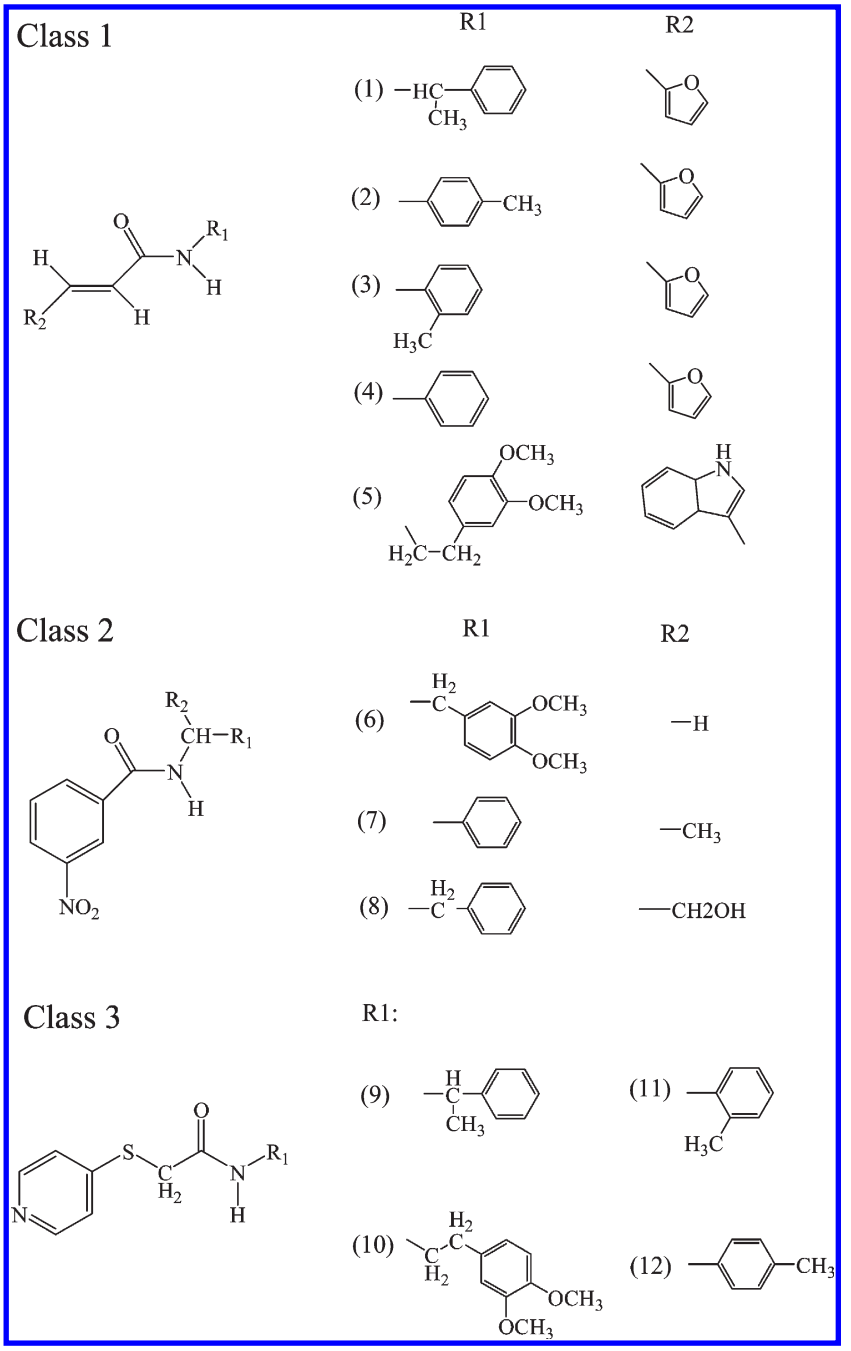

Figure 1. Molecular structures of compounds **1**−**12**. The chemical names are 3-furan-2-yl-*N*-(1-phenylethyl)acrylamide (compound **1**), 3-furan-2-yl-*N*-*p*-tolylacrylamide (compound **2**), 3-furan-2-yl-*N*-*o*-tolylacrylamide (compound **3**), 3-furan-2-yl-*N*-phenylacrylamide (compound **4**), *N*-[2-(3,4-dimethoxyphenyl)ethyl]-3-(1*H*-indol-3-yl)acrylamide (compound **5**), *N*-[2-(3,4-dimethoxyphenyl)ethyl]-3-nitrobenzamide (compound **6**), 7,3-nitro-*N*-(1-phenylethyl)benzamide (compound **7**), *N*-(1-benzyl-2-hydroxyethyl)-3-nitrobenzamide (compound **8**), *N*-(1-phenylethyl)-2-(pyridin-4-ylsulfanyl)acetamide (compound **9**), *N*-[2-(3,4-dimethoxyphenyl)ethyl]-2-(pyridin-4-ylsulfanyl)acetamide (compound **10**), 2-(pyridin-4-ylsulfanyl)-*N*-*o*-tolylacetamide (compound **11**), and 2-(pyridin-4-ylsulfanyl)-*N*-*p*-tolylacetamide (compound **12**).

(reviewed in refs 7−9). PAMs include a wide range of compounds that enhance the activity of agonists, and some of them display receptor specificity. Among PAMs, we can differentiate those that do not change the AChR desensitization properties (type I) from those that decrease the level of desensitization (type II). At least three possible PAM binding sites were previously studied (reviewed in refs 7−9): the extracellular subunit interface domain characterized for galantamine,[10] the site located in the middle of the transmembrane helices characterized for PNU-120596,[11] and the site at the extracellular−transmembrane junction characterized for NS-1738.[12]

In this work, we first synthesized a series of novel amide derivatives (see Figure 1 for molecular structures) with potential AChR activity and subsequently characterized them by applying chemical, structural, and functional approaches, including spectroscopic methods, Ca^{2+} influx-induced fluorescence detection,

dx.doi.org/10.1021/bi102001m |*Biochemistry* 2011, 50, 5263–5278

radioligand binding assays using noncompetitive antagonists such as [^{3}H]TCP ([*piperidyl*-3,4-^{3}H(N)]-{*N*-[1-(2-thienyl)-cyclohexyl]-3,4-piperidine}) and agonist and/or competitive antagonists, including [^{3}H]epibatidine, [^{3}H]cytisine, and [^{3}H]-methyllycaconitine ([^{3}H]MLA),[13] and molecular docking and dynamics simulations.

EXPERIMENTAL PROCEDURES

Materials. [^{3}H]Epibatidine (45.1 Ci/mmol), [^{3}H]cytisine (35.6 Ci/mmol), [^{3}H]TCP ([*piperidyl*-3,4-^{3}H(N)]-{*N*-[1-(2-thienyl)cyclohexyl]-3,4-piperidine}, 45.0 Ci/mmol), and [^{3}H]-imipramine (47.5 Ci/mmol) were obtained from PerkinElmer Life Sciences Products, Inc. (Boston, MA). [^{3}H]Methyllycaconitine ([^{3}H]MLA, 100 Ci/mmol) was purchased from American Radiolabeled Chemicals Inc. (St. Louis, MO). The radioligands were stored at −20 °C. Methyllycaconitine citrate, carbamylcholine dichloride (CCh), imipramine hydrochloride, polyethylenimine, leupeptin, bacitracin, pepstatin A, aprotinin, benzamidine, phenylmethanesulfonyl fluoride, sucrose, sodium azide, and thyrotropin-releasing hormone (TRH) amide were purchased from Sigma Chemical Co. (St. Louis, MO). α-Bungarotoxin (α-BTx) was purchased from Invitrogen Co. (Carlsbad, CA). [1-(Dimethylamino)naphthalene-5-sulfonamido]ethyltrimethylammonium perchlorate (dansyltrimethylamine) was purchased from Pierce Chemical Co. (Rockford, IL). (±)-Epibatidine hydrochloride, Geneticin, and hygromycine B were obtained from Tocris Bioscience (Ellisville, MO). Fetal bovine serum (FBS) and trypsin/EDTA were purchased form Gibco BRL (Paisley, U.K.). Ham's F-12 nutrient mixture was obtained from Invitrogen (Paisley, U.K.). Phencyclidine hydrochloride (PCP) was obtained through the National Institute on Drug Abuse (NIDA, National Institutes of Health, Baltimore, MD). All chemicals used for the synthesis of compounds **1**−**12** were obtained from Chenzhuo Co. (Zhengzhou, China). Salts were of analytical grade. Solvents were purified and dried by standard procedures.

Synthesis of Compounds 1−12. A series of novel amide derivatives (see the molecular structures of compounds **1**−**12** in Figure 1) were synthesized by the coupling reaction between carboxylic acid and the corresponding aryl or fatty amines catalyzed by *N*,*N*′-2-dicyclohexylcarbodiimide (DCC) and 4-(dimethylamino)pyridine (4-DMAP) based on previous work.[14,15] Carboxylic acid (1.1 mmol), DCC (1.1 mmol), and 4-DMAP (0.08 mmol) were dissolved in anhydrous dichloromethane (5 mL), and the solution was cooled to 0 °C and stirred for 30 min. Then, a solution of amine (1.0 mmol) in dichloromethane (5 mL) was added dropwise over 15 min. When the addition was complete, the mixture corresponding to compounds **1**−**7** was warmed to room temperature (RT) and stirred for 12 h, whereas the mixture corresponding to compounds **8**−**12** was refluxed for 6 h and then cooled to RT. *N*,*N*′-Dicyclohexylurea was filtered off, and the solvent was removed under reduced pressure. The residue was purified by flash silica gel chromatography using an ethyl acetate/petroleum ether mixture (1:3, v/v) to give the expected product.

Structural and Chemical Characterization of Compounds 1−12. The uncorrected melting point of each compound was measured using a WC-1 microscopic apparatus (Keyi Co.). Infrared spectra were recorded on a Bruker VECTOR22 spectrophotometer (Bruker Daltonik GmbH, Bremen, Germany) using KBr pellets. ^{1}H NMR and ^{13}C NMR spectra were recorded using a Bruker DTX-400 spectrometer (Bruker Daltonik GmbH). Samples were dissolved in $CDCl_3$ and placed in 5 mm NMR tubes. Measurements were taken using a $CDCl_3$ lock and tetramethylsilane as an internal reference.

Mass spectra were recorded in positive ion mode using a Bruker ESQUIRE 3000 ion trap spectrometer (Bruker Daltonik GmbH, Fällanden, Switzerland) equipped with a gas nebulizer probe, capable of analyzing ions up to m/z 6000. Nitrogen was used as the drying gas at a flow rate of 4.5 L/min. The nebulizer pressure was 7.5 psi. The capillary was typically held at 4 kV, and the source temperature was maintained at 300 °C. The instrument was operated at unit-mass resolution, and the calibration of m/z was performed using a standard ES-tuning-mix. The samples were continuously infused into the ESI chamber by a Cole-Parmer 74900 syringe pump (Cole Parmer Instrument Co., Vernon Hills, IL). Measurements and calculations are based on the mass of the most abundant isotopes.

The high-resolution mass spectral data were recorded on a Bruker APEXII Fourier transform ion cyclotron resonance (FTICR) MS instrument (Bruker Daltonik GmbH) with an external ion source and analyzed using liquid secondary ion (LSI) MS with a Cs ion gun in positive ion mode. The accelerating voltage of the ion gun was 10 kV, and the acquisition range was from m/z 100 to 600. The sample was introduced as methanolic solutions.

Compound ***1*** *[3-furan-2-yl-N-(1-phenylethyl)acrylamide]:* ^{1}H NMR ($CDCl_3$, 400 MHz) δ 1.55 (d, 3H, J = 7.2 Hz), 5.25−5.30 (m, 1H), 5.90 (bs, 1H), 6.3 (d, 1H, J = 12 Hz), 6.44 (s, 1H), 6.53 (s, 1H), 7.35−7.43 (m, 7H); ^{13}C NMR ($CDCl_3$, 400 MHz) δ 165.0, 151.3, 143.9, 143.2, 128.6, 128.0, 127.9, 127.3, 126.2, 118.5, 118.4, 113.6, 112.0, 48.9, 21.7; HRMS calcd for $C_{15}H_{15}NO_2$ + MS 241.1, found 241.7; HRMS calcd for $C_{15}H_{15}NO_2$ − MS 240.1, found 239.7; mp 149−151 °C; yield 69.6%.

Compound ***2*** *(3-furan-2-yl-N-p-tolylacrylamide):* ^{1}H NMR ($CDCl_3$, 400 MHz) δ 2.32 (s, 3H), 6.45 (d, 1H), 6.51 (s, 1H), 6.55 (d, 1H), 7.12 (d, 2H), 7.52 (d, 2H), 7.43 (s, 1H), 7.47 (m, 1H), 7.63 (s, 1H); ^{13}C NMR ($CDCl_3$, 400 MHz) δ 163.9, 151.3, 144.5, 144.2, 130.2, 129.5, 128.7, 120.0, 118.8, 114.7, 114.2, 112.3, 112.2, 20.9; HRMS calcd for $C_{14}H_{13}NO_2$ + MS 227.1, found 227.7; HRMS calcd for $C_{14}H_{13}NO_2$ − MS 226.1, found 225.7; mp 142−144 °C; yield 82.0%.

Compound ***3*** *(3-furan-2-yl-N-o-tolylacrylamide):* ^{1}H NMR ($CDCl_3$, 400 MHz) δ 2.31 (s, 3H), 6.48−6.51 (m, 2H), 6.60 (d, 1H), 7.12 (s, 2H), 7.20−7.21 (m, 2H), 7.47−7.56 (t, 2H), 7.98 (s, 1H); ^{13}C NMR ($CDCl_3$, 400 MHz) δ 166.8, 154.0, 151.3, 151.2, 144.5, 144.2, 130.5, 130.1, 126.7, 117.00, 114.6, 114.4, 112.2, 17.8; HRMS calcd for $C_{14}H_{13}NO_2$ + MS 227.1, found 227.7; mp 138−140 °C; yield 94.1%.

Compound ***4*** *(3-furan-2-yl-N-phenylacrylamide):* ^{1}H NMR ($CDCl_3$, 400 MHz) δ 1.63−1.64 (d, 3H), 5.30−5.37 (q, 1H), 6.68−6.69 (d, 1H), 7.28−7.31 (m, 1H), 7.34−7.41 (m, 4H), 7.60−7.64 (t, 1H), 8.14−8.16 (d, 1H), 8.31−8.34 (d, 1H), 8.58 (s, 1H); ^{13}C NMR ($CDCl_3$, 400 MHz) δ 164.2, 148.1, 142.5, 136.1, 133.3, 129.8, 128.8, 127.7, 126.3, 126.0, 121.7, 49.7, 21.5; HRMS calcd for $C_{15}H_{14}N_2O_3$ + MS 270.1, found 270.8; HRMS calcd for $C_{15}H_{14}N_2O_3$ − MS 269.1, found 268.8; mp 144−146 °C; yield 69.6%.

Compound ***5*** *{N-[2-(3,4-dimethoxyphenyl)ethyl]-3-(1H-indol-3-yl)acrylamide}:* ^{1}H NMR ($CDCl_3$, 400 MHz) δ 2.82−2.86 (t, 2H), 3.65−3.66 (d, 2H), 3.77 (t, 3H), 3.82 (s, 3H), 6.11 (s, 1H), 6.41−6.45 (d, 2H), 6.71−6.79 (m, 3H), 7.13−7.21

(m, 3H), 7.34−7.35 (s, 1H), 7.39−7.41 (d, 1H), 7.83−7.90 (q, 2H), 9.69 (s, 1H); ^{13}C NMR ($CDCl_3$, 400 MHz) δ 167.7, 148.9, 147.6, 137.3, 134.9, 131.5, 128.5, 125.3, 122.8, 121.0, 120.7, 120.1, 115.5, 113.1, 112.0, 111.4, 55.9, 55.8, 41.0, 35.4; HRMS calcd for $C_{21}H_{22}N_2O_3S$ + MS 350.2, found 350.9; mp 159−161 °C; yield 60.2%.

Compound ***6*** *{N-[2-(3,4-dimethoxyphenyl)ethyl]-3-nitrobenzamide}:* ^{1}H NMR ($CDCl_3$, 400 MHz) δ 2.89−2.92 (t, 2H), 3.70−3.75 (q, 2H), 3.84 (s, 6H), 6.56 (s, 1H), 6.76−6.83 (q, 3H), 7.59−7.63 (t, 1H), 8.08−8.10 (d, 1H), 8.30−8.33 (t, 1H), 8.51 (s, 1H); ^{13}C NMR ($CDCl_3$, 400 MHz) δ 165.1, 149.1, 148.1, 147.8, 136.2, 133.1, 131.0, 129.8, 125.9, 121.6, 120.7, 111.8, 111.4, 55.8, 55.8, 41.5, 35.0; HRMS calcd for $C_{17}H_{18}N_2O_5$ + MS 330.1, found 330.8; HRMS calcd for $C_{17}H_{18}N_2O_5$ − MS 229.1, found 328.8; mp 141−143 °C; yield 80.4%.

Compound ***7*** *[7,3-nitro-N-(1-phenylethyl)benzamide]:* ^{1}H NMR ($CDCl_3$, 400 MHz) δ 1.63−1.64 (d, 3H), 5.30−5.37 (q, 1H), 6.68−6.69 (d, 1H), 7.28−7.31 (m, 1H), 7.34−7.41 (m, 4H), 7.60−7.64 (t, 1H), 8.14−8.16 (d, 1H), 8.31−8.34 (d, 1H), 8.58 (s, 1H); ^{13}C NMR ($CDCl_3$, 400 MHz) δ 164.2, 148.1, 142.5, 136.1, 133.3, 129.8, 128.8, 127.7, 126.3, 126.0, 121.7, 49.7, 21.5; HRMS calcd for $C_{15}H_{14}N_2O_3$ + MS 270.1, found 270.8; HRMS calcd for $C_{15}H_{14}N_2O_3$ − MS 269.1, found 268.8; mp 144−146 °C; yield 69.6%.

Compound ***8*** *[N-(1-benzyl-2-hydroxyethyl)-3-nitrobenzamide]:* ^{1}H NMR ($CDCl_3$, 400 MHz) δ 3.0 (d, 2H, J = 8 Hz), 3.74 (d, 1H), 3.84 (d, 1H), 4.43 (bs, 1H), 6.55 (s, 1H), 7.25−7.30 (m, 4H), 7.35 (t, 2H), 7.63 (t, 1H), 8.07 (d, 1H, J = 8 Hz), 8.33−8.36 (m, 1H), 8.50 (s, 1H); ^{13}C NMR ($CDCl_3$, 400 MHz) δ 165.3, 148.1, 137.3, 136.0, 133.1, 129.8, 129.2, 128.8, 126.9, 126.1, 121.7, 63.6, 53.3, 36.9; HRMS calcd for $C_{16}H_{16}N_2O_4$ + MS 300.1, found 300.8; HRMS calcd for $C_{16}H_{16}N_2O_4$ − MS 299.1, found 298.7; mp 133−135 °C; yield 72.4%.

Compound ***9*** *[N-(1-phenylethyl)-2-(pyridin-4-ylsulfanyl)-acetamide]:* ^{1}H NMR ($CDCl_3$, 400 MHz) δ 1.40−1.42 (d, 3H), 3.69 (s, 2H), 5.08−5.11 (t, 1H), 6.89−6.90 (d, 1H), 7.07−7.13 (m, 4H), 7.23−7.25 (d, 3H), 8.39−8.40 (d, 2H); ^{13}C NMR ($CDCl_3$, 400 MHz) δ 165.7, 149.6, 146.4, 142.3, 128.6, 127.5, 125.9, 120.5, 49.1, 49.0, 34.6, 21.4; HRMS calcd for $C_{15}H_{16}N_2OS$ + MS 273.1, found 272.8; HRMS calcd for $C_{15}H_{16}N_2OS$ − MS 271.1, found 270.8; mp 125−127 °C; yield 17.6%.

Compound ***10*** *{N-[2-(3,4-dimethoxyphenyl)ethyl]-2-(pyridin-4-ylsulfanyl)acetamide}:* ^{1}H NMR ($CDCl_3$, 400 MHz) δ 2.68−2.71 (t, 2H), 3.49−3.54 (q, 2H), 3.65 (s, 2H), 3.83−3.85 (d, 6H), 6.52−6.54 (q, 1H), 6.62−6.68 (q, 3H), 7.03−7.04 (q, 2H), 8.41−8.42 (d, 2H); ^{13}C NMR ($CDCl_3$, 400 MHz) δ 166.5, 149.5, 149.0, 147.7, 146.6, 130.5, 120.5, 111.6, 111.2, 55.8, 55.8, 40.9, 34.8, 34.5; HRMS calcd for $C_{17}H_{20}N_2O_3S$ + MS 333.1, found 332.9; mp 109−110 °C; yield 23.7%.

Compound ***11*** *[2-(pyridin-4-ylsulfanyl)-N-o-tolylacetamide]:* ^{1}H NMR ($CDCl_3$, 400 MHz) δ 2.02 (s, 3H), 3.83 (s, 2H), 7.03−7.12 (m, 2H), 7.14−7.17 (m, 3H), 7.66−7.68 (d, 1H), 8.40−8.41 (d, 2H), 8.55−8.40 (s, 1H); ^{13}C NMR ($CDCl_3$, 400 MHz) δ 164.9, 149.5, 146.5, 134.7, 130.5, 129.3, 126.8, 125.8, 122.8, 120.5, 35.2, 17.2; HRMS calcd for $C_{14}H_{14}N_2OS$ + MS 259.1, found 258.8; mp 121−123 °C; yield 31.6%.

Compound ***12*** *[2-(pyridin-4-ylsulfanyl)-N-p-tolylacetamide]:* ^{1}H NMR ($CDCl_3$, 400 MHz) δ 2.31 (s, 3H), 3.83 (s, 2H), 7.11−7.17 (t, 2H), 7.18−7.19 (t, 2H), 7.33−7.35 (d, 2H), 8.32 (s, 1H), 8.45−8.46 (q, 2H); ^{13}C NMR ($CDCl_3$, 400 MHz) δ 164.9, 149.7, 146.4, 134.8, 134.4, 129.5, 120.5, 120.2, 35.4, 20.8; HRMS calcd for $C_{14}H_{14}N_2OS$ + MS 258.1, found 258.8; mp 128−129 °C; yield 29.1%.

Cell Culture Procedures. The source and cell culture procedures for the HEK293-hα3β4 and HEK293-hα4β2 cells,[16−18] as well as for the GH3-hα7, SHSY5Y-hα7,[17,19] and TE671-hα1β1$\gamma\delta$ (human rhabdomyosarcoma cell line obtained from American Type Culture Collection)[16,20] cell lines, were the same as previously described. HEK293-hα3β4, HEK293-hα4β2, and TE671-hα1β1$\gamma\delta$ cells were cultured in a 1:1 mixture of Dulbecco's modified Eagle's medium containing 3.7 g/L $NaHCO_3$, 1.0 g/L sucrose, supplemented with stable glutamine (L-alanyl-L-glutamine, 524 mg/L), and Ham's F-12 nutrient mixture containing 1.176 g/L $NaHCO_3$ and supplemented with 10% (v/v) FBS, Geneticin (0.2 mg/mL), and hygromycine B (0.2 mg/mL). GH3-hα7 cells were cultured in Ham's F-12 nutrient mixture with 1.176 g/L $NaHCO_3$ and stable glutamine, supplemented with 10% (v/v) FBS and 50 μg/mL Geneticin. SHSY5Y-hα7 cells were cultured in Dulbecco's modified Eagle's medium supplemented with 10% (v/v) FBS and 100 μg/mL Geneticin. All cells were cultured at 37 °C, 5% CO_2, and 95% relative humidity and passaged every 3 days by being detached from the cell culture flask and washed with phosphate-buffered saline and brief incubation (~3 min) with trypsin (0.5 mg/mL) and EDTA (0.2 mg/mL).

AChR Membrane Preparation. To prepare cell membranes in large quantities, we used the method of Arias et al.[17−19] Briefly, SH-SY5Y-hα7, HEK293-hα4β2, and HEK293-hα3β4 cells were cultured separately in suspension using nontreated Petri dishes (150 mm × 15 mm). After being cultured for ~3 weeks, cells were harvested by being gently scraped and centrifuged at 1000 rpm for 5 min at 4 °C using a Sorvall Super T21 centrifuge. Cells were resuspended in binding saline (BS) buffer [50 mM Tris-HCl, 120 mM NaCl, 5 mM KCl, 2 mM $CaCl_2$, and 1 mM $MgCl_2$ (pH 7.4)], containing 0.025% (w/v) sodium azide and a cocktail of protease inhibitors, including leupeptin, bacitracin, pepstatin A, aprotinin, benzamidine, and phenylmethanesulfonyl fluoride. The suspension was maintained on ice and homogenized using a Polytron PT3000 instrument (Brinkmann Instruments Inc., Westbury, NY) and then centrifuged at 10000 rpm for 30 min at 4 °C. The pellet was finally resuspended in BS buffer containing 20% sucrose (w/v) using the Polytron and briefly (6 × 15 s) sonicated (Branson Ultrasonics Co., Danbury, CT) to ensure maximal homogenization.

Torpedo AChR native membranes were prepared from frozen *Torpedo californica* electric organs obtained from Aquatic Research Consultants (San Pedro, CA) by differential and sucrose density gradient centrifugation, as described previously.[21] The numbers of AChR binding sites on these membrane preparations were determined by the decrease in dansyltrimethylamine (6.6 μM) fluorescence produced by the titration of suberyldicholine into receptor suspensions (0.3 mg/mL) in the presence of 100 μM PCP that ranged from 1.0 to 1.2 nmol of suberyldicholine binding sites/mg of total protein (0.5−0.6 nmol of AChR/mg of protein). Total protein was determined using the bicinchoninic acid protein assay (Thermo Fisher Scientific, Rockford, IL). The AChR membrane preparations were stored at −80 °C in 20% sucrose until they were required.

Ca^{2+} Influx Measurements in Cells Containing Different AChR Subtypes. Ca^{2+} influx was assessed essentially as previously described.[16−20] Briefly, GH3-hα7, HEK293-hα4β2, HEK293-hα3β4, and TE671-hα1β1$\gamma\delta$ cells were seeded 48 h prior to the experiment on black 96-well plates (Costar) at a

density of 5×10^4 cells/well and incubated at 37 °C in a humidified atmosphere (5% CO_2/95% air). For the HEK293-hα4β2, HEK293-hα3β4, and TE671-hα1β1γδ cells, the medium was changed to 1% bovine serum albumin (BSA) in a HEPES-buffered salt solution (HBSS) [130 mM NaCl, 5.4 mM KCl, 2 mM $CaCl_2$, 0.8 mM $MgSO_4$, 0.9 mM NaH_2PO_4, 25 mM glucose, and 20 mM HEPES (pH 7.4)] 16−24 h before the experiment. On the day of the experiment, the medium was removed by flicking the plates and replaced with 100 μL of HBSS with 1% BSA containing 2 μM Fluo-4 (Molecular Probes, Eugene, OR) in the presence of 2.5 mM probenecid (Sigma, Buchs, Switzerland). The cells were then incubated at 37 °C in a humidified atmosphere (5% CO_2/95% air) for 1 h. Plates were flicked to remove excess Fluo-4, washed twice with HBSS, and then placed in the cell plate stage of the fluorimetric imaging plate reader (Molecular Devices, Sunnyvale, CA). For the TE671 cells, NMG buffer was used in this step. This buffer is a modified HBSS buffer containing *N*-methyl-D-glucamine instead of NaCl, KH_2PO_4 as the replacement for NaH_2PO_4, and 4.5 mM KCl instead of 5.4 mM KCl. To measure agonistic activities of compounds **1**−**12**, the plate was refilled with 100 μL of HBSS, and then different concentrations of each compound were injected while the fluorescence was recorded for 3 min. To measure the PAM activity of all compounds or the antagonistic activity of compounds **1**−**4** (class 1), **7** (class 2), and **12** (class 3), each compound was added at the concentrations indicated in the figures instead of the second washing step and each mixture preincubated for 5 min at RT. Thereafter, (±)-epibatidine (0.1 μM for hα4β2, hα3β4, and hα7 AChRs and 1.0 μM for the hα1β1γδ AChR) was added from the agonist plate to the cell plate using the 96-tip pipettor, and the fluorescence was recorded for 3 min. To determine the inhibitory mechanism of these compounds at hα3β4 AChRs, additional experiments were performed by preincubating the cells with 3, 10, and 30 μM compound **4**, before the addition of 0.1 μM (±)-epibatidine. To further study the pharmacological activity of compounds **1**−**4**, GH3-hα7 cells were treated with 20 nM (±)-epibatidine containing increasing concentrations of each compound. To further investigate whether the PAM activity of the compounds depends on the binding of the agonist to the receptor, 0.4 μM MLA was used. For the thyrotropin-releasing hormone (TRH) amide experiments, cells were pretreated with 20 μM **2**−**4** followed by stimulation with TRH amide. For all measurements, a baseline consisting of five measurements of 0.4 s each was recorded. The laser excitation and emission wavelengths were 488 and 510 nm, respectively, at 1 W, with a CCD camera opening of 0.4 s.

The concentration−response data were curve-fitted, and the IC_{50}, apparent EC_{50}, Hill coefficient (n_H), and efficacy (E_{max}) values were calculated by nonlinear least-squares analysis using Prism (GraphPad Software, San Diego, CA).

Radioligand Binding Experiments. To determine whether compounds **1**−**4** modulate the binding of a radioligand to the AChR agonist sites, the effect of these compounds on binding of [^{3}H]MLA to hα7 AChRs, on binding of [^{3}H]epibatidine to hα7 and hα3β4 AChRs, and on binding of [^{3}H]cytisine to hα4β2 and *Torpedo* AChRs was determined as described previously.[19] To determine whether these compounds bind to the AChR ion channel, additional [^{3}H]TCP and [^{3}H]imipramine competition binding experiments were performed. The [^{3}H]-TCP experiments were performed using *Torpedo* AChRs in the absence (resting but activatable state) and presence of 1 μM α-BTx (resting state) or 1 mM CCh (desensitized state).[20,22] α-Bungarotoxin is a competitive antagonist that maintains the AChR in the resting (closed) state.[23] AChR membranes (0.5−1.5 mg/mL) were suspended in BS buffer with 4.1 nM [^{3}H]-MLA, 6.9 nM [^{3}H]epibatidine, 8.7 nM [^{3}H]cytisine, 12 nM [^{3}H]TCP, or 17 nM [^{3}H]imipramine and preincubated for 30 min (or 5 min for the [^{3}H]epibatidine binding to the hα7 AChR) at RT. The used initial radioligand concentrations give high specific binding activity and low noise as demonstrated previously.[17−22] The total volume was divided into aliquots, and increasing concentrations of each compound were added to each tube and incubated for 90 min (or for 20 min for [^{3}H]epibatidine binding to the hα7 AChR) at RT. Nonspecific binding was assessed in the presence of 10 μM MLA (or 1 μM α-BTx) ([^{3}H]-MLA experiments), 1 mM CCh ([^{3}H]cytisine experiments), 1 μM (±)-epibatidine (or 1 mM CCh) ([^{3}H]epibatidine experiments), 100 μM PCP ([^{3}H]TCP experiments), and 100 μM imipramine ([^{3}H]imipramine experiments). The AChR-bound radioligand was then separated from the free radioligand by a filtration assay using a 48-sample harvester system with GF/B Whatman filters (Brandel Inc., Gaithersburg, MD), previously soaked with 0.5% polyethylenimine for 30 min. The membrane-containing filters were transferred to scintillation vials with 3 mL of Bio-Safe II (Research Product International Corp., Mount Prospect, IL), and the radioactivity was determined using a Beckman LS6500 scintillation counter (Beckman Coulter, Inc., Fullerton, CA). The concentration−response data were curve-fitted, and the apparent EC_{50}, n_H, and maximal binding (B_{max}) values were calculated by nonlinear least-squares analysis using Prism.

Homology Modeling of the hα3β4, hα4β2, and hα7 AChRs. The extracellular domain from each AChR subtype was constructed by homology modeling methods based on the crystal structure of the *Aplysia* acetylcholine binding protein (AChBP) [Protein Data Bank (PDB) entry 2byq].[24] First, the amino acid sequences of the extracellular domain from each AChR subunit, including the α7 (i.e., residues 26−230), α3 (i.e., residues 34−240), β4 (i.e., residues 27−232), α4 (i.e., residues 37−243), and β2 (i.e., residues 29−234) subunits,[25] were aligned with that for the AChBP using ClustalX2.[26] Then, homology models of the hα7, hα3β4, and hα4β2 AChRs were constructed using MODELER 9.[27] To maintain the symmetry of the pentamers, symmetry constraints were imposed on the Cα atoms of the five hα7 subunits and the two α (i.e., α3 and α4) and two β (i.e., β2 and β4) subunits from the respective hα3β4 and hα4β2 AChRs. Energy minimization was used to refine the three-dimensional (3D) structures of the homology models. Then, each AChR with the highest MODELER score was used in further docking studies. The 3D structure of the whole hα7 AChR was constructed by the same method based on the structure of the α1 subunit from the *Torpedo* AChR (PDB entry 2BG9).[28]

Molecular Docking and Molecular Dynamics Simulations. To define the most probable binding site for the compounds with PAM activity (i.e., compounds **2**−**4**), compound **2** was first docked to potential PAM binding sites on the hα7 AChR. Three possible PAM binding sites were studied (reviewed in refs 7−9): the extracellular domain site characterized for galantamine,[10] located at the subunit interface ∼12 Å from the agonist binding site, the site characterized for PNU-120596 located in the middle of the transmembrane helices,[11] and the site characterized for NS-1738 located at the extracellular−transmembrane junction.[12] The compounds were first put manually in the vicinity of each

PAM binding site, and the docking simulations were performed with AutoDock4.0.[29] One hundred independent runs were performed in a cubic box of 40 Å × 40 Å × 40 Å by genetic algorithms,[29] and the conformations with the lowest binding energies at each binding site were used for further dynamics simulations. To evaluate the stability of the predicted conformations of the ligand when bound to each of the three different sites, 10 ns molecular dynamics simulations were performed on the hα7 AChR−compound **2** complex using the GROMACS package.[30] To save simulation time, the simulations at the extracellular−transmembrane junction were performed using only the residues within 20 Å of compound **2** bound to its locus (Figure 5D). For the simulations at the interfacial domain, two subunits containing the extracellular domain were used (Figure 5B), whereas only one subunit containing the four transmembrane helices was used in the simulation at the transmembrane domain (Figure 5C). Because we want to observe only the stability of the PAMs, the Cα atoms were constrained to preserve the 3D structure of the proteins. To determine whether compounds **2**−**4** bind to any of the three potential PAM sites at the hα3β4 and hα4β2 AChRs, additional docking and molecular dynamics simulations were performed using compound **2**. To determine the required structural components for the observed specificity of compounds **2**−**4** for the hα7 AChR, each compound was docked to the postulated PAM site at the hα7 AChRs.

The other simulation parameters were similar to those used in our previous studies.[19] The complexes were put in a dodecahedron box and solvated by single-point charge water molecules. Na^+ ions were added as counterions to neutralize the simulation system by replacing the water molecules randomly. Berendsen's algorithm[31] was used to keep the system at a constant temperature and a constant pressure, and the particle mesh Ewald method[32,33] was used to calculate the long-range electrostatic interactions. A cutoff of 1.4 Å was used to account for the van der Waals interactions as previously explained.[19]

Calculation of the Root-Mean-Square Deviation Values of Compound 2. The conformations of the AChR−PAM complexes were extracted every 10 ps from the simulation trajectory and superposed with the initial structure by least-squares fitting of the atoms of the protein. Then, the root-mean-square deviation (rmsd) values of compound **2** were calculated with the following equation:

$$\mathrm{rmsd} = \sqrt{\frac{1}{N}\sum_{i=1}^{N}\delta_i^{\,2}} \qquad (1)$$

where N is the number of atoms in compound **2** and δ_i is the distance between the corresponding atoms of compound **2** from each snapshot compared with that from the starting conformation. Thus, the rmsd values represent not only the intermolecular conformational changes but also the rotation and transition of the whole molecule.

Physicochemical Characterization of Compounds 1−12. For the structural characterization of compounds **1**−**12**, several physicochemical parameters, including the solvent accessible surface area (SASA), hydrophobic SASA, polar SASA, hydrophobicity (i.e., logP), and molecular volume, were calculated. The SASA, hydrophobic SASA, and polar SASA were calculated by using the Visual Molecular Dynamics (VMD) package,[34] whereas the logP and molecular volume were calculated by using Molinspiration (http://www.molinspiration.com).

Scheme 1. Reaction Mechanism for Compounds 1−12[a]

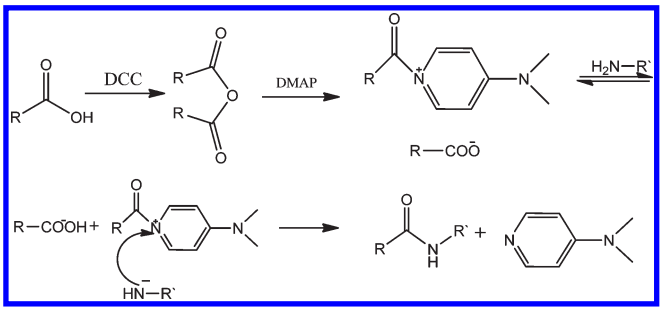

[a] See Figure 1 for molecular structures. In this mechanism, the carboxylic acid is converted to anhydride by DCC, which forms an acylpyridinium species with the catalyst (i.e., DMAP). This is followed by equilibration of the acylpyridinium species with the amine to produce ion pairs. The nucleophilic attack produced by R′-NH^- on the acyl group from the ion pair generates the amide group and the catalyst. The carboxylic acid is then recycled by DCC, while the catalyst is reused in the formation of acylpyridinium species.

RESULTS

Chemical Characterization of Compounds 1−12. A series of novel amide derivatives were synthesized by the coupling reaction between carboxylic acid and the corresponding aryl or fatty amines catalyzed by both DCC and 4-DMAP. We found that the addition of 3−10 mol % 4-DMAP accelerates the DCC-activated *N*-acylureas of carboxylic acids with amines to such an extent that the formation of side products is suppressed and even sterically demanding amides are formed in good yields.

The mechanism of synthesis is shown in Scheme 1. In this mechanism, the carboxylic acid is converted to anhydride by DCC, which forms an acylpyridinium species with the catalyst.[35] This is followed by equilibration of acylpyridinium species with the amine to produce ion pairs. The nucleophilic attack produced by RN^- on the acyl group from the ion pair generates the amide group and the catalyst. The carboxylic acid is then recycled by DCC, while the catalyst is reused in the formation of acylpyridinium species.

The chemical structure of each compound (see Figure 1) was characterized by ^{1}H NMR, ^{13}C NMR, and MS spectral analyses. ESI mass spectra for all compounds showed the $[M + H]^+$ ion, suggesting that the structures of title compounds are reasonable. Because the basic structure of compounds **1**−**12** was similar (see also the structural differences among them in the next section), compound **2** was chosen as an example to explain their chemical characteristics. In the ^{1}H NMR spectrum (not shown), two doublet peaks at 7.52 and 7.12 ppm were assigned to the protons on the benzene ring, because of their interaction with each other. A singlet peak for methanyl group protons was observed at 2.32 ppm. Two singlet peaks at 6.51 and 7.43 ppm were assigned to the protons on the furan ring. A broad singlet peak at 7.63 ppm was assigned to the amide protons.

Structural Characterization of Compounds 1−12. The structural scaffold of compounds **1**−**12** (see Figure 1) is based on a benzene ring connected by an amide linkage to another aromatic moiety (e.g., furan, benzyl, and pyridine rings). According to the chemical group connected to the carboxylic carbon, these molecules can be divided into three different classes (Figure 1). Class 1 compounds have a double bond connecting the carbonyl group and the furan (compounds **1**−**4**) or indole

Table 1. Physicochemical Parameters for Compounds 1−12[a]

compound	class	solvent accessible surface area (Å^2)	hydrophobic solvent accessible surface area (Å^2)	polar solvent accessible surface area (Å^2)	logP	VdW (Å^3)
1	1	466.0	398.9	67.1	2.81	229.2
2		473.9	401.7	72.2	2.99	212.4
3		447.6	370.9	76.7	2.95	212.4
4		448.2	371.7	76.5	2.55	195.8
5		660.9	534.9	126.0	3.19	327.9
6	2	583.0	411.5	171.5	2.52	294.9
7		486.3	352.3	134.0	3.02	243.6
8		543.0	355.0	188.0	2.23	268.6
9	3	430.9	356.4	74.5	2.15	251.0
10		501.5	404.6	96.9	1.64	302.3
11		398.2	307.4	90.8	2.29	234.2
12		432.4	324.5	107.9	2.33	234.1

[a] The solvent accessible surface area (SASA), hydrophobic SASA, and polar SASA values of compounds **1**−**12** were calculated using the VMD package,[34] whereas the logP and VdW (molecular volume) values were calculated using Molinspirstion (http://www.molinspiration.com).

(compound **5**) ring. Class 2 compounds have the carbonyl group directly linked to the benzyl ring, and class 3 compounds have a CH_2-S connection between the carbonyl group and the pyridine ring.

The SASA, hydrophobic SASA, polar SASA, hydrophobicity (i.e., logP), and molecular volume values for each compound are listed in Table 1. In general, compounds from class 1 have smaller molecular volumes than those for the other classes. For example, compounds **2**−**4** have smaller molecular volumes (195−212 Å^3) than compound **5** (∼330 Å^3), whereas they have values in the same range as those for compounds **1**, **11**, and **12** (229−234 Å^3). Class 1 compounds also have smaller polar SASA values than members of the other classes. However, compounds **1**−**4** have values (67−77 Å^2) in the same range as that for compound **9** (74.5 Å^2). Although class 1 compounds have in general logP values (2.55−3.19) larger than that for the other compounds, the values for compounds **6** (2.52) and **7** (3.02) are in the same range. This correlates very well, as expected, with the hydrophobic SASA values, where the values for class 1 compounds (371−535 Å^2) are larger than that for the other compounds, with the exception of compounds **6** (412 Å^2) and **10** (405 Å^2). Finally, no trend among classes was observed for the SASA values.

Pharmacological Activity and Specificity of Compounds 1−12. The pharmacological activity of compounds **1**−**12** (see molecular structures in Figure 1) was first determined by Ca^{2+} influx experiments using hα7 AChR-containing cells. The results indicate that compounds **1**−**12** do not have agonistic activity on hα7 AChRs (Figure 2A). However, both the potency and the efficacy of (±)-epibatidine were increased by pretreating the cells with 20 μM compounds **2**−**4** (Figure 2B). On the other hand, compounds **1** and **5**−**12** exhibited neither antagonistic nor PAM activity on the hα7 AChR up to 100 μM. The PAM activity elicited by compounds **2**−**4** was completely obliterated by the presence of 400 nM MLA (see the empty symbols in Figure 2B), a selective hα7 AChR antagonist.[13] To determine the apparent EC_{50} values for the PAM activity of compounds **2**−**4**, cells were pretreated with different concentrations of the compound and challenged with an EC_{50} concentration of (±)-epibatidine (i.e., 20 nM) (see Figure 2C). The calculated apparent EC_5 values are in the ∼5 μM concentration range (see Table 2). The compounds also increased the (±)-epibatidine efficacy (ΔE_{max}) by ∼2-fold (see Table 2). The observed n_H values for the PAM activity are higher than unity (see Table 2), indicating that this interaction is mediated by a cooperative mechanism. This type of mechanism fits very well with the concept of positive modulation, where one molecule (i.e., PAM) enhances the activity of a second molecule (i.e., agonist).

To determine whether the observed ligand-induced Ca^{2+} influx enhancement (see Figure 2B,C) is due to a positive allosteric modulation of the hα7 AChR and not due to an unspecific increase in the level of intracellular Ca^{2+}, GH3-α7 cells were stimulated with TRH amide as studied previously.[36] TRH amide activates the endogenously expressed Gq protein-coupled receptor, triggering a transient cytoplasmic Ca^{2+} increase. Compounds **2**−**4** do not change the TRH amide-elicited Ca^{2+} transient (Figure 2D), indicating that these PAMs do not directly modulate release of Ca^{2+} from intracellular stores.

The pharmacological activity of compounds **1**−**4** (class 1), **7** (class 2), and **12** (class 3) (see Figure 1) was further investigated on the hα4β2 (Figure 3A), hα3β4 (Figure 3B,C), and hα1β1γδ (Figure 3D) AChRs, respectively. None of the compounds displayed agonistic or PAM activity at these AChRs; rather, most of the compounds behave as antagonists of the (±)-epibatidine-elicited Ca^{2+} influx. Depending on the studied compound, the calculated IC_{50} values are in the 28−65, 12−90, and 18−118 μM concentration ranges for the hα4β2, hα3β4, and hα1β1γδ subtypes, respectively, where compound **2** is the most active (Table 2). Figure 3C also shows that the inhibitory action is mediated by a noncompetitive mechanism. In summary, these results demonstrate that the PAM activity of compounds **2**−**4** is selective for the hα7 AChR, and that these compounds also behave as noncompetitive antagonists of the hα4β2, hα3β4, and hα1β1γδ AChRs.

Radioligand Binding Experiments. To determine whether compounds **2**−**4** bind to the hα7 AChR agonist binding sites, we performed additional radioligand binding assays. The results indicate that compounds **2**−**4** do not inhibit binding of [^{3}H]-MLA to hα7 AChRs (Figure 4A). Nevertheless, these compounds enhance binding of [^{3}H]epibatidine to hα7 AChRs (Figure 4B), where the efficiency for compound **2** was higher than that for compounds **3** and **4** (Table 3). Considering the apparent EC_{50} values (Table 3), we demonstrate that compound

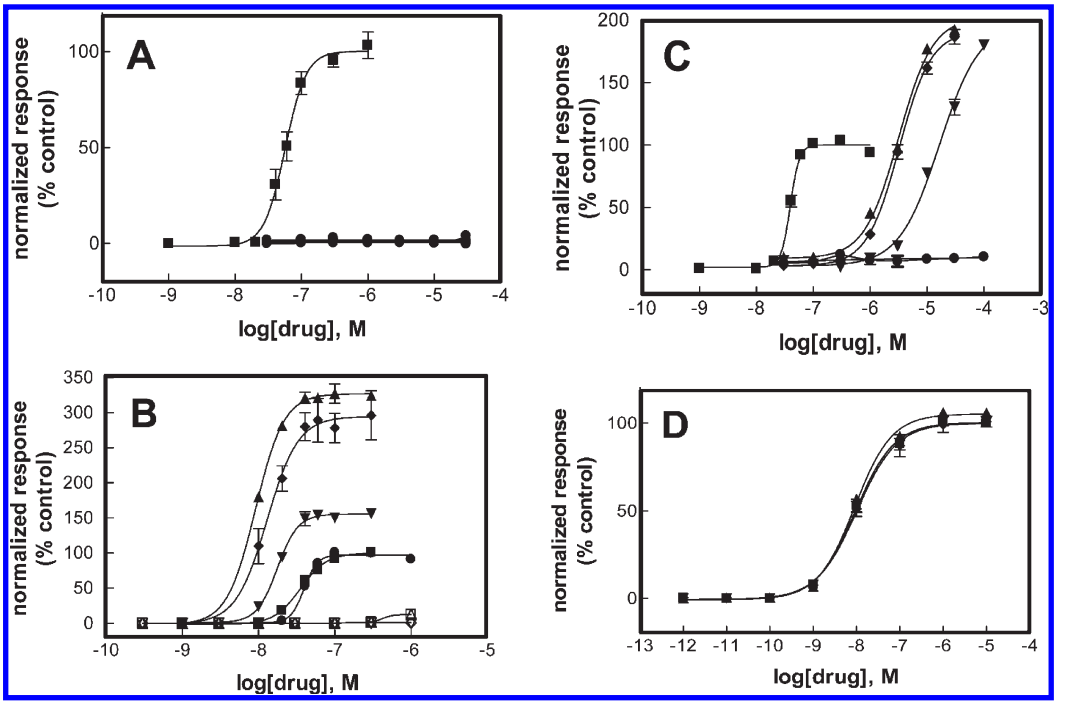

Figure 2. Functional effects of compounds **1**−**12** on GH3-hα7 cells. (A) Increased concentrations of (±)-epibatidine (■), but not of compounds **1**−**12** (●), increase the intracellular level of Ca^{2+}, suggesting that these compounds are not agonists of hα7 AChRs. (B) Compound **2** (▲), **3** (▼), or **4** (◆) at 20 μM, but not compound **1** (●), enhances (±)-epibatidine-induced Ca^{2+} influx (■). The agonistic activity of (±)-epibatidine (□) and the PAM activity of compounds **2** (△), **3** (▽), and **4** (◇) are inhibited by 400 nM MLA. (C) Increased concentrations of compounds 2 (▲), **3** (▼), and **4** (◆), but not compound **1** (●), enhance the agonistic activity elicited by 20 nM (±)-epibatidine [i.e., the EC_5 concentration for (±)-epibatidine]. The calculated apparent EC_{50}, n_H, and E_{max} (in percent) values are summarized in Table 2. (D) Lack of an effect of PAMs on GPCR-mediated Ca^{2+} signaling in GH3-hα7 cells. Compounds **2** (▲), **3** (▼), and **4** (◆) at 20 μM do not change the effect elicited by TRH amide (■) on intracellular Ca^{2+}. The plots are representative of ten (■) and four (●, ▲, ▼, ◆, △, ◇, and ▽) determinations, where the error bars represent the standard deviation.

3 has practically the same potency as compound **2**, but both are more potent than compound **4**. Because compound **1** did not exhibit PAM activity (Table 2), its effect on binding of [^{3}H]epibatidine to hα7 AChRs was also determined as a negative control. As expected, compound **1** did not enhance [^{3}H]epibatidine binding, supporting the functional results (Table 2).

Because compounds **2**−**4** exhibited inhibitory activity on hα4β2, hα3β4, and hα1β1γδ AChRs (Figure 3A−D and Table 2), additional radioligand binding experiments were performed to determine the inhibitory mechanism. The [^{3}H]epibatidine and [^{3}H]cytisine binding results indicate that compounds **2** and **4** do not bind to the agonist and/or competitive antagonist binding sites on the hα4β2 (Figure 4C), hα3β4 (Figure 4D), and *Torpedo* α1β1γδ AChRs. These results support the results of the Ca^{2+} influx experiments (see Figure 3C), indicating that the observed inhibition is mediated by a noncompetitive mechanism. Because a noncompetitive mechanism can be mediated by a luminal interaction, we tested whether these compounds bind to the [^{3}H]TCP and [^{3}H]imipramine binding sites in the AChR ion channel. The [^{3}H]TCP competition binding results using the *Torpedo* AChR indicate that compound **4** does not bind to the PCP site located within the desensitized and resting AChR ion channels (Figure 4E). Similar experiments with the resting hα4β2 and hα3β4 AChRs also suggest that compound **2** does not interfere with binding of [^{3}H]-imipramine to the ion channels (Figure 4F). The result using the *Torpedo* AChR in the resting but activatable state also shows that compound **4** does not modulate the interaction of [^{3}H]TCP with the AChR ion channel (Figure 4E). This indicates that these compounds produce no conformational change in the vicinity of the TCP site when the ion channel is in the resting state.

PAM Binding Site Location at the hα7 AChR Suggested by Molecular Dynamics Simulations. The molecular interactions between compounds **2**−**4** and several possible PAM binding sites at the hα7 AChR (reviewed in refs 7−9) were studied by molecular dynamics. One of these PAM binding sites is potentially located at the extracellular subunit interface ~12 Å from the agonist site.[10,37] Other potential PAM binding sites lie in the middle of the four transmembrane helices[11] and at the extracellular−transmembrane junction.[12] To investigate which binding site is the most probable for the PAMs in this study, compound **2** was first docked to each of the three possible PAM sites on the hα7 AChR. Ten nanosecond dynamics simulations at 300 K were performed to subsequently evaluate the stability of compound **2** bound to the respective PAM sites on the hα7 AChR. The molecular dynamics simulations indicate that compound **2** moved away from its initial position in the transmembrane domain and at the extracellular−transmembrane junction during the 10 ns simulation (Figure 5C,D), whereas it binds to the interfacial domain in a steady manner (Figure 5B). The larger rmsd values (~0.8 nm) for the transmembrane domain and the extracellular−transmembrane junction compared to that for the interfacial domain (~0.2 nm) (see Figure 5A) also indicate that compound **2** is more stable when it binds to the interfacial domain. Because our simulations indicate that compound **2** binds to only the subunit interface domain in a steady manner, we propose that the interfacial binding site at the extracellular domain is the most probable locus for these PAMs. A distance of ~12 Å between the PAM and agonist sites was estimated by calculating the

Table 2. Pharmacological Properties of Compounds 1−12 on Several AChR Subtypes Assessed by Ca^{2+} Influx Assays

AChR subtype	compound	PAM activity apparent EC_{50} (μM)[a]	n_H[c]	ΔE_{max}[a] (%)
hα7	**2**	4.6 ± 0.9	1.74 ± 0.14	104 ± 13
	3	24.8 ± 7.2	2.14 ± 0.45	130 ± 23
	4	5.5 ± 1.5	1.89 ± 0.28	112 ± 10
	1 and **5**−**12**	none	not available	not available
AChR subtype	compound	antagonistic activity apparent IC_{50} (μM)[b]	n_H[c]	ΔE_{max}[a] (%)
hα4β2	**1**	83 ± 25	0.99 ± 0.12	not available
	2	28 ± 6	1.16 ± 0.13	
	3	60 ± 21	1.67 ± 0.33	
	4	44 ± 16	1.47 ± 0.09	
	7	65 ± 1	1.02 ± 0.14	
	12	>100	not available	
hα3β4	**1**	30 ± 5	1.77 ± 0.36	not available
	2	12 ± 2	2.30 ± 0.06	
	3	32 ± 9	2.06 ± 0.23	
	4	14 ± 4	1.84 ± 0.19	
	7	90 ± 21	1.01 ± 0.14	
	12	46 ± 18	1.65 ± 0.42	
hα1β1γδ	**1**	65 ± 11	1.87 ± 0.23	not available
	2	18 ± 2	2.30 ± 0.41	
	3	39 ± 3	1.86 ± 0.23	
	4	34 ± 3	1.92 ± 0.36	
	7	72 ± 8	1.88 ± 0.23	
	12	118 ± 52	1.44 ± 0.20	

[a] Values were obtained from Figure 2A−C, in the presence of 20 nM (±)-epibatidine. [b] Values were obtained from Figure 3A,B,D. [c] Hill coefficient.

distance between the center of mass of compound **2** bound to the PAM site and the center of mass of (+)-epibatidine bound to the agonist site (see Figure 6B). On the other hand, molecular dynamics simulations suggest that these three binding sites are not probable for compound **2** at the hα3β4 and hα4β2 AChRs (see Figures S3 and S4 of the Supporting Information). Molecular dynamics results also suggest that compound **2** does not bind to the agonist and/or competitive antagonist site of the hα7, hα3β4, and hα4β2 AChRs (see Figure S1 of the Supporting Information). This result is consistent with the experimental data indicating that these compounds inhibit ion flux of hα3β4 and hα4β2 AChRs by noncompetitive mechanisms (see Figure 3C).

Structural Elements Responsible for PAM Binding and Receptor Selectivity Predicted by Molecular Docking. To determine the structural components underlying the observed receptor specificity for the PAM activity elicited by compounds **2**−**4**, we compared the docking of these compounds at the hα7/α7, hα4/β2, and hα3/β4 interfaces. To investigate why compounds **2**−**4** are PAMs whereas compounds **1** and **5**−**12** are not, the 12 ligands were docked to the PAM site in the hα7−α7 interface. Figure 6B shows the most probable location of the PAM binding site at the interface of two hα7 subunits, ∼12 Å from the agonist binding site (center-to-center distance). The PAM binding site at the hα7−α7 interface (Figure 6B−D and Figure S2A of the Supporting Information) and its homologues at the hα3−β4 (Figure S2B of the Supporting Information) and hα4−β2 (Figure S2C of the Supporting Information) interfaces present slight but important differences. Panels A and D of Figure 6 show the residues involved in the PAM site at the hα7−α7 interface based on the docking results. The most important residues involved in the interaction with compounds **2**−**4** include Val19 (in the pre-β1 strand), Trp83 (in the β3−β4 loop), Lys84 (in the β3−β4 loop), Asp86 (in the β3−β4 loop), and Tyr148 (in the β7−β8 loop; although this loop is also known as loop B for the agonist site, the residues for the PAM site are different) located on the (+) face, and Pro78 (in the β3−β4 loop), His102 (in the β5−β5′ loop), and Asn104 (in the β5−β5′ loop) located on the (−) face. This result will help in the design of future single-mutation experiments to test what residues are important for PAM binding and activity. The main structural differences between the PAM binding sites from distinct AChR subtypes are mutation of α7-His102 to Tyr104 on the β2 and β4 subunit (−) faces and α7-Lys84 to α4-Arg84 on the (+) face (Figure S2 of the Supporting Information).

The docking results indicate that the benzene rings from compounds **2**−**4** are well aligned within the postulated PAM locus, forming hydrophobic interactions with Pro78 from the α7, β4, and β2 (−) faces and with Val19 from the α7, α3, and α4 (+) faces. The amide group contributes with additional hydrogen bond interactions, which seem to be comparatively more important for PAM activity. As shown in Figure S2A−C of the Supporting Information, compound **2** forms hydrogen bonds with both (+) and (−) faces of the hα7 AChR. However, hydrogen bonds are only found on the (+) faces of the postulated PAM sites in the hα3β4 and hα4β2 AChRs (described in the Supporting Information).

Another important difference among the AChR subtypes is the size of the PAM locus. We propose that the pharmacological difference observed between the hα7 AChR and the hα3β4 and hα4β2 AChRs with respect to the PAM activity elicited by

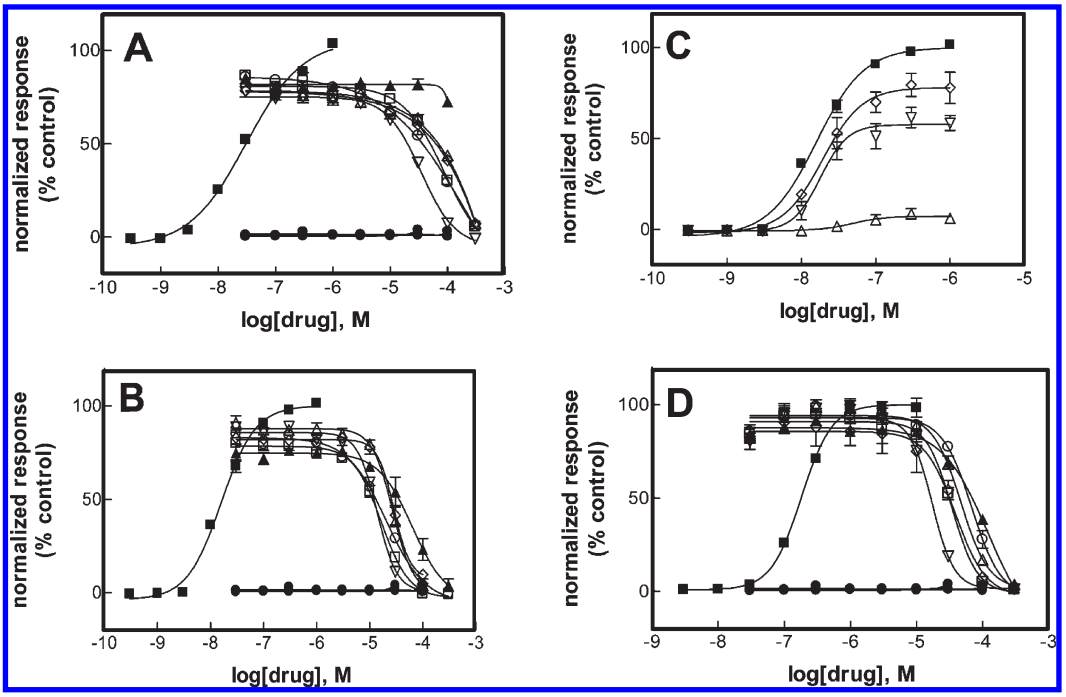

Figure 3. Functional effect of compounds **1**−**4**, **7**, and **12** on (A) HEK293-hα4β2, (B and C) HEK293-hα3β4, and (D) TE671-hα1β1γδ cells using Ca^{2+} influx measurements. (A, B, and D) Increased concentrations of (±)-epibatidine (■), but not of compounds **1**−**4** (as examples of class 1), **7** (as an example of class 2), and **12** (as an example of class 3) (●), increase the intracellular level of Ca^{2+}, suggesting that these compounds are not agonists of the studied AChRs. The inhibitory effect of compounds **1** (△), **2** (▽), **3** (◇), **4** (□), **7** (○), and **12** (▲) was investigated after pretreating (5 min) cells with different concentrations of each compound followed by activation of the receptor with (±)-epibatidine (■, 100 nM for HEK293-hα4β2 and HEK293-hα3β4 cells and 1 μM for TE671-hα1β1γδ cells). (C) Pretreatment with 3 (◇), 10 (▽), or 30 μM compound **4** (△) inhibits (±)-epibatidine (■)-elicited hα3β4 activation in a dose-dependent and noncompetitive manner. The plots are representative of 10 (■) and 3−5 (●, △, ▽, ◇, □, ○, and ▲) determinations, where the error bars represent the standard deviation. The ligand response was normalized to the maximal (±)-epibatidine response, which was set to 100%. The calculated IC_{50} and n_H values for these compounds are summarized in Table 2.

compounds **2**−**4** can be ascribed to the natural mutation of α7-His102 to β2/β4-Tyr104. Because Tyr has a side chain larger than that of His, this mutation results in a smaller binding site in hα3β4/hα4β2 AChRs compared with that in the hα7 AChR. Thus, steric hindrance between β2/β4-Tyr104 and the furan ring of compounds **2**−**4** is found, which may be responsible for their subtype specificity (Figure S2A−C of the Supporting Information). In conclusion, the steric hindrance of the Tyr105 residue as well as the smaller number of hydrogen bonds may be responsible for the experimental results showing that compounds **2**−**4** are PAMs on the hα7 AChR but have no PAM activity on the hα3β4 and hα4β2 AChRs.

The benzene ring of compound **1** is aligned in the same conformation as that for compounds **2**−**4** in the PAM locus (Figure S2A,D of the Supporting Information). However, the amide group of compound **1** is shifted away (Figure S2A,D of the Supporting Information) because of the steric hindrance mediated by the methyl group located between the amide and benzene groups (Figure 1). Thus, one of the hydrogen bonds between the amide group of compounds **2**−**4** and the hα7-Asn104 side chain is nonexistent in the hα7 AChR−compound **1** complex (Figure S2A,D of the Supporting Information). These results explain the experimental results indicating that whereas compounds **2**−**4** are PAMs of the hα7 AChR, compound **1** does not behave as a PAM and emphasize the importance of concerted ligand interactions.

Similar results are found when compounds **6**−**8** [class 2 (see Figure 1)] were docked to the PAM binding site of the hα7 AChR (Figure S2E of the Supporting Information). Although these molecules are in conformations similar to those for compounds **2**−**4**, no hydrogen bond is found between the amide group and the residues in the PAM binding site because of an additional methyl (compound **7**) or ethyl (compounds **6** and **8**) group located between the benzene ring and the amide group (see Figure 1).

When compounds **9**−**12** [class 3 (see Figure 1)] were docked to the hα7 AChR PAM site, they exhibit a quite different conformation with respect to compounds **2**−**4** (Figure S2F of the Supporting Information). The sulfide atom is responsible for the different binding conformation because the relatively small bond angle between the two S−C bonds [between the sulfide atom and the methyl group and the pyridine ring (see Figure 1)] forces the pyridine ring to bend, increasing the volume of this moiety. In fact, the molecular volume of class 3 compounds (230−300 $Å^3$) is larger than that for compounds **2**−**4** (195−212 $Å^3$) (see Table 1). Thus, it is likely that compounds **9**−**12** cannot interact properly with the PAM site because of the observed steric hindrance.

In conclusion, the amide group of compounds **2**−**4** has proven to be an important pharmacophore for PAM activity by forming hydrogen bonds with both faces of the postulated PAM site. In the case of compounds **1** and **6**−**8**, which are not PAMs, the hydrogen bonds are not formed because of the existence of an additional short alkyl group between the amide group and the benzene ring (see Figure 1). The sulfide atom of compounds **9**−**12** forces the molecule to bend, producing steric hindrance at

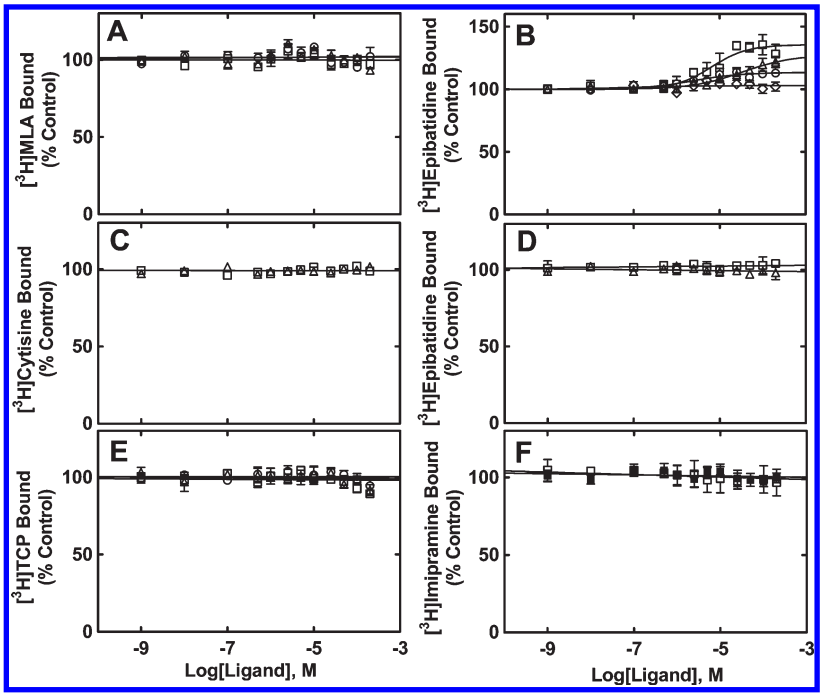

Figure 4. Effect of compounds **1** (◇), **2** (□), **3** (○), and **4** (△) on binding of a radioligand to different AChRs. The competition experiments were (A) binding of [^{3}H]MLA and (B) binding of [^{3}H]epibatidine to hα7 AChRs, (C) binding of [^{3}H]cytisine to hα4β2 AChRs, (D) binding of [^{3}H]epibatidine to hα3β4 AChRs, (E) binding of [^{3}H]TCP to *Torpedo* AChRs, and (F) the effect of compound **2** on binding of [^{3}H]imipramine to hα4β2 (□) and hα3β4 (■) AChRs. (E) The [^{3}H]TCP binding experiments for compound **4** were performed in the absence of any ligand [resting but activatable state (○)] and in the presence of 1 μM α-BTx [resting state (△)] or 1 mM CCh [desensitized state (□)]. AChR membranes were preincubated with 4.1 nM [^{3}H]MLA, 6.9 nM [^{3}H]epibatidine, 8.7 nM [^{3}H]cytisine, 12 nM [^{3}H]TCP, and 17 nM [^{3}H]imipramine and then equilibrated with increasing concentrations of the ligand under study. Nonspecific binding was assessed at 10 μM MLA (hα7 AChR), 1 mM CCh (hα4β2 AChR), 1 μM (±)-epibatidine (hα3β4 AChR), 100 μM PCP ([^{3}H]TCP experiments), and 100 μM imipramine ([^{3}H]imipramine experiments). Each plot is the combination of two to three separate experiments each performed in triplicate, where the error bars correspond to the standard deviation. The apparent EC_{50}, n_H, and B_{max} (percent) values were obtained by nonlinear least-squares fit and are summarized in Table 3.

Table 3. Modulatory Activity of Compounds 1−4 on Binding of a Radioligand to hα7 AChRs

		[^{3}H]epibatidine binding		
compound	[^{3}H]MLA binding	apparent EC_{50}[a] (μM)	n_H[b]	ΔB_{max}[a] (%)
1	–	no enhancement	–	–
2	no effect	6.5 ± 3.7	1.20 ± 0.37	30 ± 3
3	no effect	2.5 ± 2.0	0.82 ± 0.49	14 ± 3
4	no effect	34 ± 24	0.74 ± 0.29	28 ± 10

[a] Apparent EC_{50} and ΔB_{max} values were calculated from Figure 4B. [b] Hill coefficients.

the PAM binding site. Finally, compound **5** is too large to fit in the PAM site.

DISCUSSION

This study is an attempt to determine the chemical, structural, binding, functional, and receptor specificity properties of a series of novel amide derivatives via comparison of their pharmacological activities on several AChR subtypes. In this regard, we applied a variety of approaches, including molecular spectroscopy, radioligand binding and Ca^{2+} influx assays, and molecular docking and dynamics studies.

The Ca^{2+} influx (see Table 2) and radioligand binding (see Table 3) results indicate that only compounds **2**−**4** from class 1 (see Figure 1) exhibit PAM activity and that this activity is specific for the hα7 AChR. Compounds **1** and **5** from class 1 and the other compounds from classes **2** and **3** do not display PAM activity on any AChR subtype (see Table 2). Comparing the molecular volumes of compounds **2**−**4** (195−212 Å^3) with that of compound **5** (∼330 Å^3) (see Table 1), we are able to infer that the large volume of compound **5** might prevent its binding to the PAM site at the hα7−α7 interface (see Figure 6) by steric hindrance. The most important structural factor contributing to its larger molecular volume is the bulky ring, which in compounds **1**−**4** is changed to the furan ring (see Figure 1). This structural feature can explain the observed lack of PAM activity of compound **5** (see Figure 2B). In this regard, we consider that the furan ring plays an important role in the PAM activity of compounds **2**−**4**. Nevertheless, because compounds **1**, **11**, and **12**, which are not PAMs (see Figure 2B), have molecular volumes

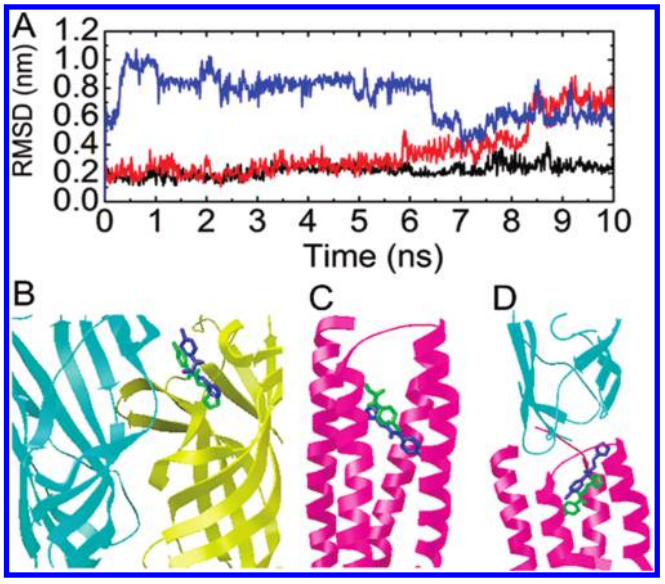

Figure 5. Molecular dynamics simulations of compound **2** at the three postulated PAM sites on the hα7 AChR. (A) rmsd values for compound **2** when it binds to the subunit interface domain (black line), to the transmembrane domain (red line), and to the extracellular−transmembrane junction domain (blue line). Location of compound **2** before (blue) and after (green) 10 ns dynamics simulations when bound to (B) the subunit interface domain, (C) the transmembrane domain, and (D) the extracellular−transmembrane junction domain. The protein is shown as ribbons, whereas compound **2** is shown as sticks. The primary [i.e., (+) face] and complementary [i.e., (−) face] components of the subunit interface are colored yellow and cyan, respectively, whereas the transmembrane segments are colored fuchsia.

similar to those for compounds **2**−**4**, additional structural characteristics must be taken into consideration. In this regard, we can rule out the possibility that hydrophobicity and polar SASA are important physicochemical properties for the PAM activity elicited by compounds **2**−**4**. This statement is based on the results indicating that although compounds **2**−**4** have logP and polar SASA values similar to those for compounds **7** and **9**, the latter compounds do not have PAM activity.

To localize the PAM binding site for compounds **2**−**4** on the hα7 AChR, we performed molecular dynamics simulations of compound **2** at the three potential PAM sites (reviewed in refs 7−9) (Figure 5). The results indicate that compound **2** is more stable when it is bound at the subunit interface site compared to that at the extracellular−transmembrane junction or at the transmembrane domain site. We also proved that compounds **2**−**4** do not bind to the agonist and/or competitive antagonist sites of the hα7, hα3β4, and hα4β2 AChRs (see Figure S1 of the Supporting Information). On the basis of this evidence, we propose that the PAM binding site for compounds **2**−**4** is located mainly in the inner β-sheet of the extracellular hα7−α7 subunit interface, ∼12 Å from the agonist site (Figure 6B). A similar location was obtained for galantamine.[10] In addition, Luttmann et al.[37] found, by using the α spheres and blind docking methods, a cavity located at a position similar to that for compounds **2**−**4**. Thus, the results from different approaches coincide with our own conclusion.

The AChR extracellular domain comprises a β-sandwich core formed by two β-sheets, the inner β-sheet containing the β1−β3, β5, β6, and β8 strands and the outer β-sheet composed of the β4, β7, β9, and β10 strands (reviewed in refs 8 and 9). The agonist binding site is formed by residues of loops A (β4−β5 loop), B (β7−β8 loop), and C (β9−β10 loop) from one subunit [known as the primary component or (+) face] and loops D (β5−β6 loop), E (β6 strand), and F (β8−β9 loop) from the other subunit [known as the complementary component or (−) face] [e.g., α4(+)/β2(−)]. It has been postulated that after agonist activation loop C adopts a close configuration and this modification triggers additional downstream conformational changes. For example, the tip of the β1−β2 linker in the inner β-sheet and the β10 strand in the outer β-sheet are displaced outward, removing the steric obstruction between the β1−β2 linker and the M2−M3 loop, which finally promotes ion channel opening (reviewed in ref 2). On the basis of the PAM locus model for the hα7 AChR (Figure 6), we propose that the interaction of these compounds with residues of the β3−β4, β5−β5′, and β7−β8 (although this loop is also known as loop B for the agonist site, the residues for the PAM site are different) loops increases the displacement of the β1−β2 linker elicited by the agonist, finally augmenting the efficacy of gating and ion channel opening processes. Our laboratory is using experimental and computational approaches to shed light on the mechanisms underlying the dual interaction between PAMs and agonists.

To determine the structural basis for the receptor specificity of compounds **2**−**4**, we docked these compounds to the respective PAM site at the hα3−β4, hα4−β2, and hα7−α7 interfaces. The docking results reveal that the amide group of compounds **2**−**4** forms hydrogen bonds with both (+) and (−) faces at the hα7−α7 interface, whereas it interacts with only the (+) face at the hα3−β4 and hα4−β2 interfaces (Figure S2A−C of the Supporting Information). This result is consistent with the fact that compounds **2**−**4** are not PAMs of hα3β4 and hα4β2 AChRs and emphasizes the concept of concerted interactions, in which the ligand must interact simultaneously with several residues to finally produce PAM activity.

In addition to the concerted ligand interactions, we propose that the observed receptor specificity for compounds **2**−**4** is also due to the mutation of hα7-His102 to hα3/hα4-Tyr104. The docking results indicate that the furan ring of compounds **2**−**4** lies between His102 and Lys84 at the hα7−α7 interface (Figure S2A of the Supporting Information). Amino acid sequence analysis indicates that residue hα7-His102 is mutated to Tyr104 in the hα3 and hα4 subunits (Figure S2B,C of the Supporting Information). Because Tyr is larger than His, the binding domain formed between the Tyr104 and Lys84/Arg84 residues at the hα3−β4 and hα4−β2 interfaces is smaller than that at the hα7−α7 interface, preventing the fitting of the furan ring within this locus (Figure S2B,C of the Supporting Information). Thus, these natural mutations may additionally explain why compounds **2**−**4** are not PAMs of the hα3β4 and hα4β2 AChRs.

Another important question is why compounds **2**−**4** are PAMs whereas the other compounds (i.e., **1** and **5**−**12**) are not. On the basis of the docking studies, we found that the amide group of compounds **2**−**4** forms hydrogen bonds with both (+) and (−) faces at the hα7−α7 interface (Figure S2A of the Supporting Information). However, the amide group of compound **1** forms a hydrogen bond with only the (+) face (Figure S2D of the Supporting Information), and no hydrogen bond is found between the amide group of compounds **6**−**8** and the PAM site (Figure S2E of the Supporting Information). The additional short alkyl group connecting the benzene ring and the

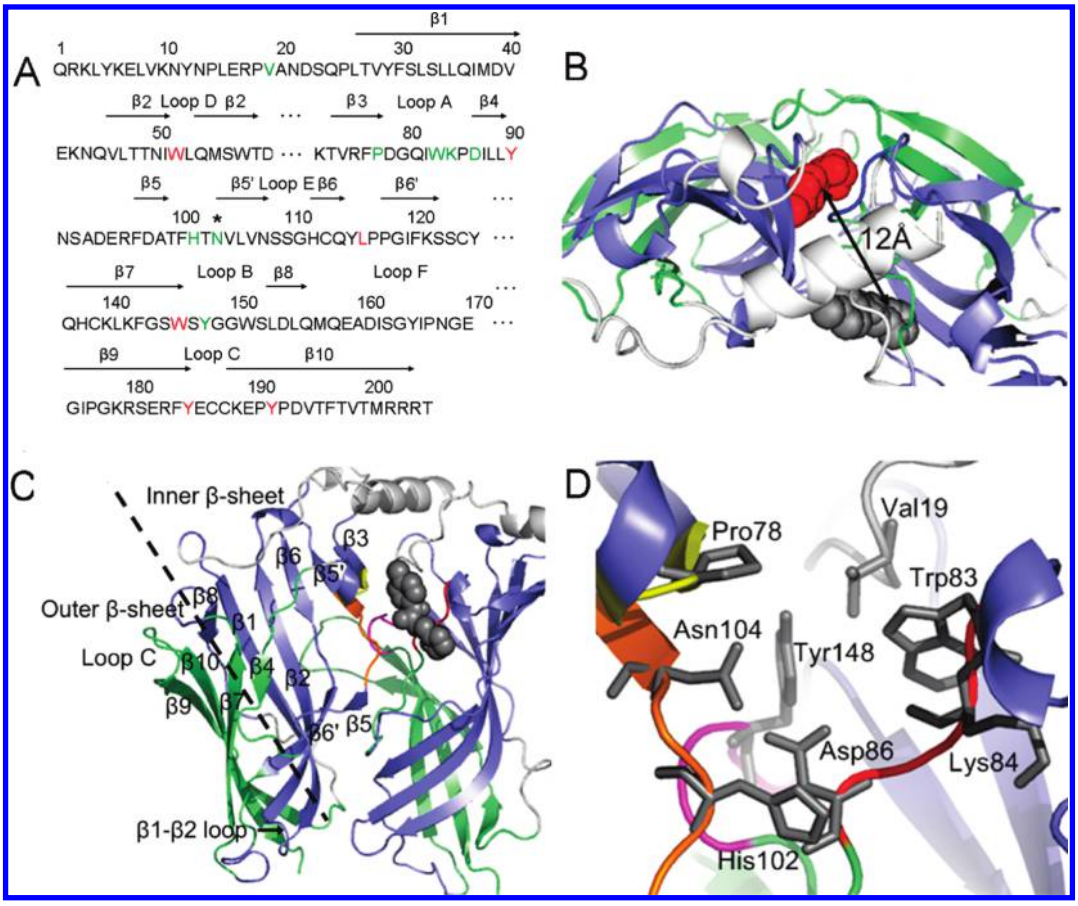

Figure 6. (A) Amino acid sequence of the hα7 subunit. Residues interacting with agonists are colored red, whereas those involved in the PAM site are colored green. Asn104, which may also indirectly interact with agonists, is labeled with an asterisk. (B) Top view of the extracellular domain of two hα7 subunits showing the interfacial location of compound **2** at the PAM binding site (gray) compared to that for (+)-epibatidine at the agonist site (red). The PAM binding site is located ~12 Å from the agonist site (center-to-center distance). The inner and outer β-sheets are colored light blue and light green, respectively. (C) Side view of the extracellular domain of two hα7 subunits showing the interfacial location of compound **2** at the PAM binding site (gray). This site is formed by two $\beta3-\beta4$ loops, one at the (+) face (red) and another at the (−) face (yellow), as well as by the $\beta5-\beta5'$ loop (orange) located in the inner β-sheet (light blue) and by the $\beta7-\beta8$ loop (magenta) located in the outer β-sheet (light green), both at the (+) face. (D) Close-up of the residues forming the PAM binding pocket at the hα7−α7 subunit interface. The residues forming the PAM locus are Trp83, Lys84, and Asp86, located in the $\beta3-\beta4$ loop on the (+) face (red); Pro78, located in the $\beta3-\beta4$ loop on the (−) face (yellow); Asn104 and His102, located in the $\beta5-\beta5'$ loop on the (+) face (orange); Tyr148, located in the $\beta7-\beta8$ loop on the (+) face (magenta); and Val19, located in the pre-$\beta1$ loop on the (+) face (gray). The other loops and β-strands of the receptor are colored light blue (inner β-sheet) and light green (outer β-sheet), respectively.

amide group found on compounds **1** and **6**−**8** is responsible for this result by shifting the amide group away. In addition, the sulfide atom on compounds **9**−**12** forces the molecule to bend, increasing its molecular volume and finally provoking steric hindrance at the PAM site (Figure S2F of the Supporting Information).

On the basis of Ca^{2+} influx (see Table 2) and radioligand binding (see Table 3) results, compounds **1**−**4** (class 1), **7** (class 2), and **12** (class 3) behave as noncompetitive antagonists of the hα4β2, hα3β4, and α1β1γδ AChRs. However, PAMs do not interact with the PCP/imipramine site or modulate [^{3}H]TCP binding within AChR ion channels (Figure 4E,F). In this regard, other potential binding sites for noncompetitive antagonists (reviewed in ref 38) might be involved. Previous results indicate that barbiturates (noncompetitive antagonists) and benzylidene−anabaseine analogues (specific α7 AChR agonists) can interact with the resting *Torpedo* ion channel, finally increasing the affinity of crystal violet[39] and [^{3}H]TCP.[22] Because we did not see this pharmacological effect, the existence of a luminal site for these PAMs in AChRs is less plausible. Instead, a negative allosteric modulator site located apart from the ion channel (reviewed in refs 8 and 9) might account for the antagonistic action elicited by these compounds. This hypothesis is supported by our molecular docking and dynamics studies indicating that these compounds do not bind to the AChR agonist sites, and although they bind to the same domain as compounds **2**−**4** in the hα7 PAM site, their interactions are structurally different from those found in the hα3β4 and hα4β2 AChR pockets (see Figure S2 of the Supporting Information).

In some cases (e.g., compounds **2** and **4**), the concentration range for the inhibitory action on the hα3β4 AChR subtype is close to that for the PAM activity on the hα7 AChR (see Table 2). Thus, both pharmacological activities could be important for future therapeutic uses. For example, a compound that enhances the action of the endogenous neurotransmitter ACh on the α7 AChR could be relevant for the treatment of diseases in which the cholinergic system is compromised as in the case of Alzheimer's disease and schizophrenia (reviewed in refs 2 and 3).

In this regard, animal studies with other PAMs with high specificity for the α7 AChR such as PNU-120596 [1-(5-chloro-2,4-dimethoxyphenyl)-3-(5-methylisoxazol-3-yl)urea],[40] SB-206553 [3,5-dihydro-5-methyl-*N*-3-pyridinylbenzo[1,2-*b*:4,5-*b*′]-dipyrrole-1(2*H*)-carboxamide],[41] A-867744 {4-[5-(4-chlorophenyl)-2-methyl-3-propionyl-1*H*-pyrrol-1-yl]benzenesulfonamide},[42] XY4083 (*N*-(4-chlorophenyl)-α-{[(4-chlorophenyl)-amino]methylene}-3-methyl-5-isoxazoleacetamide),[43] and NS-1738 [1-(5-chloro-2-hydroxyphenyl)-3-(2-chloro-5-trifluoromethylphenyl)urea][44] indicated that these compounds improve the symptoms of schizophrenia in mutant mice or those provoked by drugs like amphetamine and dizocilpine (reviewed in refs 2 and3). Some of these compounds can also improve cognition (e.g., PNU-120596 and NS-1738) and attention (e.g., XY4083) in animals (reviewed in refs 2 and 3). This experimental evidence supports the view that these PAMs, as well as compounds **2**−**4**, might be potentially used for the therapy of schizophrenia and Alzheimer's disease. In addition, compounds inhibiting the α4β2 and α3β4 AChRs might have antidepressant activity and could be used for the treatment of drug addiction[17,18] (reviewed in refs 4, 9, 45, and 46). This dual allosteric activity will be very beneficial for Alzheimer's disease patients with significant depression, which is observed in more than 20% of the cases.[47] An example of dual activity is the drug 522-054, which has both positive (on α7 AChRs) and negative (on α5-GABA$_A$Rs) allosteric properties in vitro and enhances animal cognition in vivo.[48] In this regard, animal studies to determine the potential therapeutic use of our novel compounds **2**−**4** are planned.

■ ASSOCIATED CONTENT

Supporting Information. Calculation methods and results describing that PAMs do not bind to the AChR agonist sites, that hydrogen bonds are important for PAM activity, that the PAM site in the hα7 AChR is larger than that in the hα3β4 and hα4β2 AChRs, and that the postulated PAM sites at the hα7 AChRs are not probable at the hα3β4 and hα4β2 AChRs. This material is available free of charge via the Internet at http://pubs.acs.org.

■ AUTHOR INFORMATION

Corresponding Author

*Luc Montagnier BioMedical Research Institute and National Key Laboratory of Microbial Metabolism, College of Life Sciences and Biotechnology, Shanghai Jiao Tong University, 800 Dongchuan Rd., Shanghai 200240, China. Telephone: 86-21-3420-4573. Fax: 86-21-3420-4573. E-mail: dqwei@sjtu.edu.cn.

Author Contributions

H.R.A. and R.-X.G. are considered first authors of this work.

Funding Sources

This research was supported by grants from the College of Pharmacy, Midwestern University (to H.R.A.), the National Basic Research Program of China (973 Program) (Contract 2011CB707500), the Chinese National Science Foundation (Contract 30870476), the National Comprehensive Technology Platforms For Innovative Drug R&D (Contract 2009ZX9301-007 to D.-Q.W.), and the Chinese National Science Foundation (Contract 20972143 to Y.Y.).

■ ACKNOWLEDGMENT

We thank the National Institute on Drug Abuse (NIDA) for the gift of phencyclidine.

■ ABBREVIATIONS

AChR, nicotinic acetylcholine receptor; AChBP, acetylcholine binding protein; ACh, acetylcholine; PAM, positive allosteric modulator; MLA, methyllycaconitine; [^{3}H]TCP, [*piperidyl*-3,4-^{3}H(N)]-{*N*-[1-(2-thienyl)cyclohexyl]}-3,4-piperidine; CCh, carbamylcholine; α-BTx, α-bungarotoxin; RT, room temperature; BS, binding saline; DCC, *N*,*N*′-2-dicyclohexylcarbodiimide; 4-DMAP, 4-(dimethylamino)pyridine; IC_{50}, ligand concentration that produces 50% inhibition of agonist-induced activation; n_H, Hill coefficient; apparent EC_{50}, ligand concentration that produces a 50% increase in the level of agonist-induced activation or binding; TRH, thyrotropin-releasing hormone; DMEM, Dulbecco's modified Eagle's medium; FBS, fetal bovine serum; rmsd, root-mean-square deviation, SASA, solvent accessible surface area.

■ REFERENCES

(1) Arias, H. R. (2006) Ligand-gated ion channel receptor superfamilies. In *Biological and Biophysical Aspects of Ligand-Gated Ion Channel Receptor Superfamilies* (Arias, H. R., Ed.) pp 1−25, Research Signpost, Kerala, India.

(2) Albuquerque, E. X., Pereira, E. F. R., Alkondon, A., and Rogers, S. W. (2009) Mammalian nicotinic acetylcholine receptors: From structure to function. *Physiol. Rev. 89*, 73–120.

(3) Romanelli, M. N., Gratteri, P., Guandalini, L., Martini, E., Bonaccini, C., and Gualtieri, F. (2007) Central nicotinic receptors: Structure, function, ligands, and therapeutic potential. *ChemMedChem 2*, 746–767.

(4) Ortells, M. O., and Arias, H. R. (2010) Neuronal networks of nicotine addiction. *Int. J. Biochem. Cell Biol. 42*, 1931–1935.

(5) Arias, H. R., Richards, V., Ng, D., Ghafoori, M. E., Le, V., and Mousa, S. (2009) Role of non-neuronal nicotinic acetylcholine receptors in angiogenesis. *Int. J. Biochem. Cell Biol. 41*, 1441–1451.

(6) Mousa, S. A., and Arias, H. R. (2010) Angiogenesis modulation by nicotine and nicotinic ligands. *J. Pediatr. Biochem. 1*, 91–104.

(7) Bertrand, D., and Gopalakrishnan, M. (2007) Allosteric modulation of α7 and α4β2 nicotinic acetylcholine receptors. *Biochem. Pharmacol. 74*, 1155–1163.

(8) Arias, H. R., and Bouzat, C. E. (2010) Activation and modulation of the nicotine receptor. *J. Pediatr. Biochem. 1*, 53–73.

(9) Arias, H. R. (2010) Positive and negative modulation of nicotinic receptors. In *Advances in Protein Chemistry and Structural Biology* (Donev, R., Ed.) Vol. 80, Chapter 5, pp 153−204, Elsevier Inc., Burlington, MA.

(10) Iorga, B., Herlem, D., Barré, E., and Guillou, C. (2006) Acetylcholine nicotinic receptors: Finding the putative binding site of allosteric modulators using the "blind docking" approach. *J. Mol. Model. 12*, 366–372.

(11) Young, G. T., Zwart, R., Walker, A. S., Sher, E., and Millar, N. S. (2008) Potentiation of α7 nicotinic acetylcholine receptors via an allosteric transmembrane site. *Proc. Natl. Acad. Sci. U.S.A. 105*, 14686–14691.

(12) Bertrand, D., Bertrand, S., Cassar, S., Gubbins, E., Li, J., and Gopalakrishnan, M. (2008) Positive allosteric modulation of the α7 nicotinic acetylcholine receptor: Ligand interactions with distinct binding sites and evidence for a prominent role of the M2-M3 segment. *Mol. Pharmacol. 74*, 1407–1416.

(13) Davies, A. R., Hardick, D. J., Blagbrough, I. S., Potter, B. V., Wolstenholme, A. J., and Wonnacott, S. (1999) Characterisation of the

binding of [^{3}H]methyllycaconitine: A new radioligand for labelling α7-type neuronal nicotinic acetylcholine receptors. *Neuropharmacology 38*, 679–690.

(14) Ma, G.-N., Zhang, Y.-P., and Shi, M. (2007) L-Proline diamides with an axially chiral binaphthylene backbone as efficient organocatalysts for direct asymmetric aldol reactions: The effect of acetic acid. *Synthesis 2*, 197–208.

(15) Neises, B., and Steglich, W. (1978) Simple method for the esterification of carboxylic acids. *Angew. Chem., Int. Ed. 17*, 522–524.

(16) Michelmore, S., Croskery, K., Nozulak, J., Hoyer, D., Longato, R., Weber, A., Bouhelal, R., and Feuerbach, D. (2002) Study of the calcium dynamics of the human α4β2, α3β4 and α1β1γδ nicotinic acetylcholine receptors. *Naunyn-Schmiedeberg's Arch. Pharmacol. 366*, 235–245.

(17) Arias, H. R., Feuerbach, D., Targowska-Duda, K. M., Russell, M. M., and Jozwiak, K. (2010) Interaction of serotonin selective reuptake inhibitors with neuronal nicotinic acetylcholine receptors in different conformational states. *Biochemistry 49*, 5734–5742.

(18) Arias, H. R., Rosenberg, A., Feuerbach, D., Targowska-Duda, K. M., Yuan, X.-J., Jozwiak, K., Moaddel, R., and Weiner, I. W. (2010) Interaction of ibogaine with human α3β4-nicotinic receptors in different conformational states. *Int. J. Biochem. Cell Biol. 42*, 1525–1535.

(19) Arias, H. R., Gu, H., Feuerbach, D., and Wei, D-Q. (2010) Different interaction between the agonist JN403 and the competitive antagonist methyllycaconitine with the human α7 nicotinic receptor. *Biochemistry 49*, 4169–4180.

(20) Arias, H. R., Rosenberg, A., Targowska-Duda, K. M., Feuerbach, D., Moaddel, R., Maciejewski, R., Jozwiak, K., Glick, S. D., and Weiner, I. W. (2010) Interaction of 18-methoxycoronaridine with muscle nicotinic receptors in different conformational states. *Biochim. Biophys. Acta 1798*, 1153–1163.

(21) Pedersen, S. E., Dreyer, E. B., and Cohen, J. B. (1986) Location of ligand-binding sites on the nicotinic acetylcholine receptor α-subunit. *J. Biol. Chem. 261*, 13735–13743.

(22) Arias, H. R., Xing, H., MacDougall, K., Blanton, M. P., Soti, F., and Kem, W. R. (2009) Interaction of benzylidene-anabaseine analogues with agonist and allosteric sites on muscle nicotinic acetylcholine receptors. *Br. J. Pharmacol. 157*, 320–330.

(23) Moore, M. A., and McCarthy, M. P. (1995) Snake venom toxins, unlike smaller antagonists, appear to stabilize a resting state conformation of the nicotinic acetylcholine receptor. *Biochim. Biophys. Acta 1235*, 336–342.

(24) Hansen, S. B., Sulzenbacher, G., Huxford, T., Marchot, P., Taylor, P., and Bourne, Y. (2005) Structures of *Aplysia* AchBP complexes with nicotinic agonists and antagonists reveal distinctive binding interfaces and conformations. *EMBO J. 24*, 3635–3646.

(25) Elliott, K. J., Ellis, S. B., Berckhan, K. J., Urrutia, A., Chavez-Noriega, L. E., Johnson, E. C., Velicelebi, G., and Harpold, M. M. (1996) Comparative structure of human neuronal α2-α7 and β2-β4 nicotinic acetylcholine receptors subunits and functional expression of the α2, α3, α4, α7, β2 and β4 subunits. *J. Mol. Neurosci. 7*, 217–218.

(26) Larkin, M. A., Blackshields, G., Brown, N. P., Chenna, R., McGettigan, P. A., McWilliam, H., Valentin, F., Wallace, I. M., Wilm, A., Lopez, R., Thompson, J. D., Gibson, T. J., and Higgins, D. G. (2007) ClustalW2 and ClustalX version 2. *Bioinformatics 23*, 2947–2948.

(27) Sali, A., and Blundell, T. L. (1993) Comparative protein modelling by satisfaction of spatial restraints. *J. Mol. Biol. 234*, 779–815.

(28) Unwin, N. (2005) Refined structure of the nicotinic acetylcholine receptor at 4 Å resolution. *J. Mol. Biol. 346*, 967–989.

(29) Morris, G. M., Goodsell, D. S., Halliday, R. S., Huey, R., Hart, W. E., Belew, R. K., and Olson, A. J. (1998) Automated docking using a Lamarchian genetic algorithm and an empirical binding free energy function. *J. Comput. Chem. 19*, 1639–1662.

(30) Lindahl, E., Hess, B., and van der Spoel, D. (2001) GROMACS: A package for molecular simulation and trajectory analysis. *J. Mol. Model. 7*, 306–317.

(31) Berendsen, H. J. C., Postma, J. P. M., DiNola, A., and Haak, J. R. (1984) Molecular dynamics with coupling to an external bath. *J. Chem. Phys. 81*, 3684–3690.

(32) Darden, T., York, D., and Pedersen, L. (1993) Particle mesh Ewald: An N-log(N) method for Ewald sums in large systems. *J. Chem. Phys. 98*, 10089–10092.

(33) Essmann, U., Perera, L., Berkowitz, M. L., Darden, T., Lee, H., and Pedersen, L. G. (1995) A smooth particle mesh ewald potential. *J. Chem. Phys. 103*, 8577–8592.

(34) Humphrey, W., Dalke, A., and Schulten, K. (1996) VMD: Visual Molecular Dynamics. *J. Mol. Graphics 14*, 33–38.

(35) Hassner, A., Strand, G., Rubenstein, M., and Patchornik, A. (1975) Levulinic esters. An alcohol protecting group applicable to some nucleosides. *J. Am. Chem. Soc. 97*, 1614–1615.

(36) Feuerbach, D., Lingenhöhl, K., Dobbins, P., Mosbacher, J., Corbett, N., Nozulak, J., and Hoyer, D. (2005) Coupling of human nicotinic acetylcholine receptors α7 to calcium channels in GH3 cells. *Neuropharmacology 48*, 215–227.

(37) Luttmann, E., Ludwig, J., Hoffle-Maas, A., Samochocki, M., Maelicke, A., and Fels, G. (2009) Structural model for the binding sites of allosterically potentiating ligands on nicotinic acetylcholine receptors. *ChemMedChem 4*, 1874–1882.

(38) Arias, H. R., Bhumireddy, P., and Bouzat, C. (2006) Molecular mechanisms and binding site locations for noncompetitive antagonists of nicotinic acetylcholine receptors. *Int. J. Biochem. Cell Biol. 38*, 1254–1276.

(39) Arias, H. R., Bhumireddy, P., Spitzmaul, G., Trudell, J. R., and Bouzat, C. (2006) Molecular mechanisms and binding site location for the noncompetitive antagonist crystal violet on nicotinic acetylcholine receptors. *Biochemistry 45*, 2014–2026.

(40) Hurst, R. S., Hajós, M., Raggenbass, M., Wall, T. M., Higdon, N. R., Lawson, J. A., Rutherford-Root, K. L., Berkenpas, M. B., Hoffmann, W. E., Piotrowski, D. W., Groppi, V. E., Allaman, G., Ogier, R., Bertrand, S., Bertrand, D., and Arneric, S. P. (2005) A novel positive allosteric modulator of the α7 neuronal nicotinic acetylcholine receptor: *In vitro* and *in vivo* characterization. *J. Neurosci. 25*, 4396–4405.

(41) Dunlop, J., Lock, T., Jow, B., Sitzia, F., Grauer, S., Jow, F., Kramer, A., Bowlby, M. R., Randall, A., Kowal, D., Gilbert, A., Comery, T. A., Larocque, J., Soloveva, V., Brown, J., and Roncarati, R. (2009) Old and new pharmacology: Positive allosteric modulation of the α7 nicotinic acetylcholine receptor by the 5-hydroxytryptamine2B/C receptor antagonist SB-206553 (3,5-dihydro-5-methyl-*N*-3-pyridinylbenzo[1,2-*b*:4,5-*b*′]dipyrrole-1(2*H*)-carboxamide). *J. Pharmacol. Exp. Ther. 328*, 766–776.

(42) Faghih, R., Gopalakrishnan, S. M., Gronlien, J. H., Malysz, J., Briggs, C. A., Wetterstrand, C., Ween, H., Curtis, M. P., Sarris, K. A., Gfesser, G. A., El-Kouhen, R., Robb, H. M., Radek, R. J., Marsh, K. C., Bunnelle, W. H., and Gopalakrishnan, M. (2009) Discovery of 4-(5-(4-chlorophenyl)-2-methyl-3-propionyl-1H-pyrrol-1-yl)benzenesulfonamide (A-867744) as a novel positive allosteric modulator of the α7 nicotinic acetylcholine receptor. *J. Med. Chem. 52*, 3377–3384.

(43) Ng, H. J., Whittemore, E. R., Tran, M. B., Hogenkamp, D. J., Broide, R. S., Johnstone, T. B., Zheng, L., Stevens, K. E., and Gee, K. W. (2007) Nootropic α7 nicotinic receptor allosteric modulator derived from $GABA_A$ receptor modulators. *Proc. Natl. Acad. Sci. U.S.A. 104*, 8059–8064.

(44) Timmermann, D. B., Grønlien, J. H., Kohlhaas, K. L., Nielsen, E. Ø., Dam, E., Jørgensen, T. D., Ahring, P. K., Peters, D., Holst, D., Christensen, J. K., Malysz, J., Briggs, C. A., Gopalakrishnan, M., and Olsen, G. M. (2007) An allosteric modulator of the α7 nicotinic acetylcholine receptor possessing cognition-enhancing properties *in vivo*. *J. Pharmacol. Exp. Ther. 323*, 294–307.

(45) Arias, H. R. (2009) Is the inhibition of nicotinic acetylcholine receptors by bupropion involved in its clinical actions?. *Int. J. Biochem. Cell Biol. 41*, 2098–2108.

(46) Arias, H. R. (2010) Molecular interaction of bupropion with nicotine acetylcholine receptors. *J. Pediatr. Biochem. 1*, 185–197.

(47) Lyketsos, C. G., Steele, C., Baker, L., Galik, E., Kopunek, S., Steinberg, M., and Warren, A. (1997) Major and minor depression in Alzheimer's disease: Prevalence and impact. *J. Neuropsychiatry Clin. Neurosci. 9*, 556–561.

(48) Gee, K. W., Johnstone, T., Hogenkamp, D. J., Yoshimura, R., Whittemore, E. R., Gu, Z., and Yakel, J. (2010) Dual allosteric modulators of neuronal nicotinic-acetylcholine and GABA-A receptors. *FASEB J. 24*, 579.5.